RETROFIT55

Ref. Ares(2025)4708131 - 12/06/2025

Funded by the European Union

Horizon Europe programme, grant agreement No. 101096068

RETROFIT SOLUTIONS TO ACHIEVE 55% GHG REDUCTION BY 2030

On board power micro-grid configurations and analysis of performances

WP 6 –Electrification and Energy Management of On-board Systems
Task 6.2 – Investigating the retrofitting of zero-carbon solutions
D6.3 – On board power micro-grid configurations and analysis of performances
Partners involved: CNR, NTUA, LJMU
Authors: Maria Carmela Di Piazza (CNR), Marcello Pucci (CNR), Onur Yuksel (LJMU), G Viknash Shagar (LJMU), Eduardo Blanco-Davis (LJMU), Juan Ahuir-Torres (LJMU), David Hitchmough (LJMU), Jin Wang (LJMU), Giulio Rodonò (CNR), John Prousalidis (NTUA), Elias Sofras (NTUA), Nikos Themelis (NTUA).

Project details

Project Title	RETROFIT SOLUTIONS TO ACHIEVE 55% GHG REDUCTION BY 2030
Project Type	Innovation Action
Project Acronym	RETROFIT55
Grant Agreement No.	101096068
Duration	36 M
Project Start Date	01/01/2023

Deliverable information

Status (F: final; D: draft; RD: revised draft)	F 12/06/2025
Planned delivery date	31/12/2024 (rescheduled to 30/06/2025)
Actual delivery date	12/06/2025
• **Dissemination level:** PU – Public, fully open, e.g. web (Deliverables flagged as public will be automatically published in CORDIS project's page) • SEN – Sensitive, limited under the conditions of the Grant Agreement • Classified R-UE/EU-R – EU RESTRICTED under the Commission Decision No2015/444 • Classified C-UE/EU-C – EU CONFIDENTIAL under the Commission Decision No2015/444 Classified S-UE/EU-S – EU SECRET under the Commission Decision No2015/444	PU
Type: Report, Website, Other, Ethics	Report

Document history

Version	Date	Created/Amended by	Changes
01	22/05/2025	CNR	First draft version
02	09/06/2025	CNR, LJMU	Updated contributions, second draft version
03	11/06/2025	Maria Carmela Di Piazza (CNR)	Third revised version
Final	12/06/2025	CNR	Final version

Quality check review

Reviewer (s)	Main changes / Actions
NTUA, CNR, LJMU	Technical revision.
Cecilia Leotardi(CNR)	Editorial revision
Cecilia Leotardi and Alessandro Iafrati (CNR)	Final review of contents and submission to EC.

Table of Contents

List of figures

List of tables

Executive Summary

This document provides analyses of different potential electrification-based retrofitting solutions focusing on the introduction of an innovative "microgrid" on the ship under study. Particularly, the study makes reference to data and operation of the M/V Kastor vessel.

The ship is envisaged to be equipped with new technologies, i.e. PTO/PTI systems, PV panels, and FC/battery/WHRS, aimed at improving energy efficiency, reducing emissions, and optimizing fuel consumption, in line with international regulations.

After outlining the key features of the electrical system of the case study vessel, the document examines the “modified” configurations of the shipboard microgrid resulting from the implementation of the identified retrofitting technologies, considering several options for both the PTO sizing criteria and for geometrical/electrical configuration of the PV array. Subsequently, in the case of PTO/PTI and integrated PV systems, an analysis is presented to estimate the impact of these technologies on the vessel’s attained EEXI value.

A substantial part of the work presented in this document pertains to an extensive analysis based on the ship’s operational data provided by the ship owner and oriented to quantitatively assess the effects of each individual technology on fuel consumption and pollutant emissions. Particularly, the analysis results in key findings on the efficiency and environmental performance of the ship implementing the PTO/PTI and integrated PV panels as retrofitting measures. The efficiency performance of hybrid fuel cell/battery/WHR-based solutions, extensively described in deliverable D6.4, are also quantified and provided in this document.

As for the PTO/PTI solution, it has been observed that a proper shaft generator design permits the reduction of the main engine’s (ME) specific fuel oil consumption (SFOC), and that the ME’s SFOC reduction is limited and does not vary significantly, thus limiting the degrees of freedom for reducing fuel consumption. In this scenario, the PTO integration implies an overall increase of the ME fuel consumption of 360 tons and an overall decrease of the diesel engine (DE) fuel consumption of 470 tons in a two-year period. This reflects on a reduction of greenhouse gas (GHG) emission by a few percentage points.

As for PV systems, their impact on the reduction of DE fuel consumption and pollutant emission (accounting for more than 20% yearly) is clearly observed. When ME consumption (not influenced by PV) is included in the calculation, this results in an overall yearly reduction of fuel consumption ranging from 3.5% to 4% and an overall yearly CO_2 reduction of about 4%.

Depending on the size of the fuel cell and batteries, as well as the type of fuel utilised in the selected fuel cell application, the integrated system comprising of the fuel cell, battery, and waste heat recovery system can significantly reduce fossil fuel consumption in DEs, thereby facilitating the elimination of emissions. Furthermore, larger plants that meet the operational demands of at least two generators using green hydrogen can decrease greenhouse gas emissions associated with electrification by over 90%.

Based on the results obtained, the proposed retrofitting solutions appear promising and worthy of further development and investigation that includes an analysis of PTO combined with an energy storage system, that is intended to be proposed and explored in the continuation of the project activities.

1 Introduction

The decarbonization of maritime transport and the enforcement of increasingly stringent international regulations on energy efficiency and environmental sustainability, such as those established by the International Maritime Organization (IMO), have underscored the urgent need to rethink and modernize onboard electrical systems. In this context, the development of advanced shipboard microgrid architectures integrating electrical retrofitting technologies emerges as a strategic priority. Among these technologies, solutions like shaft generators (PTO/PTI systems) and photovoltaic (PV) panels stand out as viable and effective solutions for enhancing the overall energy efficiency of vessels while simultaneously reducing their environmental footprint. As a matter of fact, they belong to a class of electrical retrofitting measures that, while not completely disrupting the original design of the ship (they can be simply integrated in the existing power/propulsion architecture), can transition it to a more efficient and greener paradigm.

The implementation of such systems introduces new design paradigms for onboard energy management, requiring the reconfiguration of traditional power distribution schemes to accommodate multiple and variable energy sources. This shift demands a comprehensive engineering approach capable of assessing not only the functional integration of these technologies, but also their operational impacts under realistic conditions.

A key aspect of this process involves the quantitative evaluation of the effects that these retrofitted electrical configurations have on performance indicators, such as the attained Energy Efficiency Existing Ship Index (EEXI), as well as on fuel consumption and pollutant emission, primarily GHG emission. Accurate sizing/configuration and data-driven analysis are essential to determine how these solutions contribute to compliance with IMO regulations and to what extent they improve the energy and environmental performance of existing vessels.

This technical investigation is particularly relevant for the retrofitting of bulk carriers and other vessel types where the integration of hybrid energy systems, comprising conventional generation units, renewable sources, and energy storage, can lead to significant operational gains. The outcomes of such studies provide critical guidance for shipowners, designers, and regulators in the pursuit of sustainable maritime operations.

Within this framework and according to the project work plan, this report presents some key findings on the most appropriate design and configuration of retrofitted shipboard microgrids tailored to the selected case study, i.e. the bulk carrier M/V Kastor ship that contains the above-mentioned technologies. Moreover, it illustrates quantitative assessments of the impact of the retrofitting technologies on the attained EEXI, which is one of the most significant design efficiency indices for ships.

Additionally, the report presents a detailed and comprehensive analysis of the effects of the proposed retrofitting technologies, including the FC/Battery/WHRS systems, as described in D6.4, utilizing the rich operational dataset related to the case study provided by the shipowner. Quantitative evaluations and precise comparisons with the baseline case are provided and discussed.

2 Report technical content

The technical contents of the report are organized as follows:

- Chapter 3 presents the current electrical system architecture of the case study vessel, the bulk carrier M/V Kastor.
- Chapter 4 discusses the various onboard microgrid configurations resulting from the implementation of systems such as PTO/PTI, PV generators, and integrated FC/battery/WHRS systems. For the PTO, several sizing options are illustrated along with their related technical implications.
- In Chapter 5, the new attained EEXI values, considering, respectively, the PTO and PV systems installed on board, are evaluated based on the procedures recommended by IMO resolutions.
- In Section 6, the effects of the proposed retrofitting solutions on the fuel consumption and emissions of the case study vessel are thoroughly analyzed, based on the ship's operational data provided by the shipowner, and the obtained results are presented.
- Section 7 presents the conclusions of this report.

3 Shipboard power system of the case study ship (M/V Kastor)

A description of the actual propulsion and electrical power supply system of the case study ship has been already given in the deliverable D6.1. It is briefly described here for the reader's convenience.

The ship's propulsion is provided by a HYUNDAI-MAN B&W main engine (ME) coupled with a single fixed pitch propeller with a diameter of 6.95 m and 5 blades.

The nameplate data of the main engine are summarized in Table 1.

The reference ship speed (V_{ref}) obtained from the approved speed-power curve calibrated to EEDI conditions based on sea trial results is equal to 13.86 knots.

The shipboard electrical power, supplying the ballast and the main engine pumps, as well as the accommodation electrical loads, is provided by a set of three identical diesel generator sets manufactured by YANMAR CO., LTD.

Technical data of the auxiliary engines (AE) and main generators (MG) are summarized respectively in Table 2 and in Table 3.

The electrical generators coupled with the auxiliary engines are connected to 440 V main switchboards from which electrical power is distributed in AC 60Hz, supplying both 440V and 220V loads located downstream of appropriate power transformers.

A simplified scheme of propulsion and electric power supply system of the M/V KASTOR ship is finally illustrated in Figure 1. It is evident that in the current configuration, propulsion and electrical power generation (and use) are inherently separated.

Table 1: Technical data of the main engine.

Manufacturer	HYUNDAY-MAN B&W
Type	6S60ME-C8.5
Maximum continuous rating (MCR_{ME})	9930 kW x 90.4 rpm
Limited maximum continuous rating with engine power limitation ($MCR_{ME,lim}$)	8230 kW
SFC at 75% of MCR_{ME} or 83% of $MCR_{ME,lim}$	166.81 g/kWh
Number of engines	1
Fuel type	MDO

Table 2: Technical data of auxiliary engines.

Manufacturer	YANMAR CO., LTD
Type	6EY22LW
Maximum continuous rating (MCR_{AE})	800 kW x 720 rpm
SFC at 50% of MCR_{AE}	215 g/kWh
Number of engines	3
Fuel type	HFO

Table 3: Technical data of main generators.

Manufacturer	YANMAR
Rated output	720 kW x 720 rpm
Voltage	AC 450 V
Number of sets	3

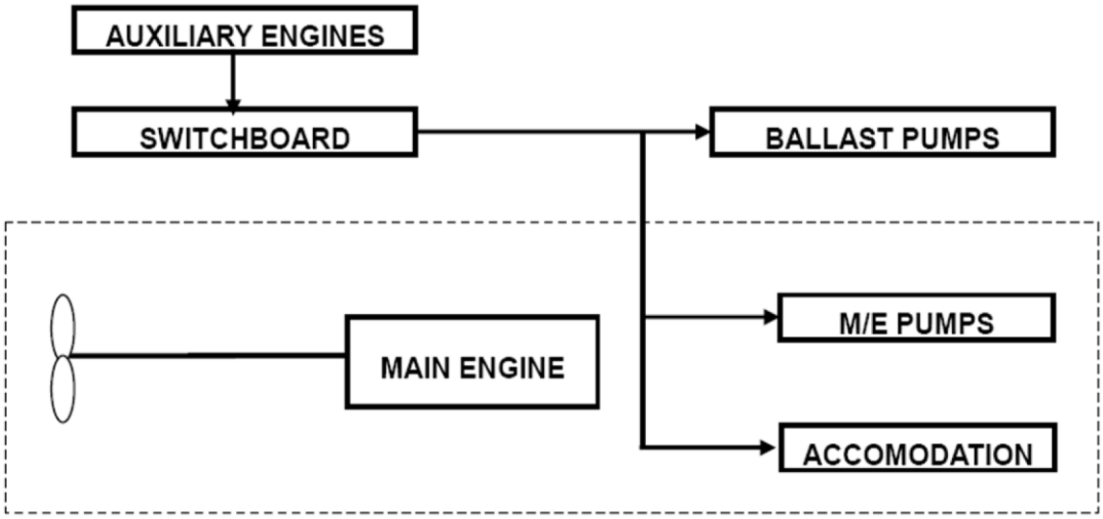

Figure 1: M/V KASTOR ship schematic figure of propulsion and electric power supply system.

4 The new shipboard microgrid configurations

Different new concepts of electrical power and propulsion systems are envisioned for the ship under study, depending on the electrification measure used for pursuing an efficiency-oriented retrofitting of the vessel. In the following, examples of PTO/PTI systems and PV panels are specially investigated, to assess their potential for efficiency increase and emission reduction. Moreover, the efficiency performance of hybrid Fuel cell/battery/WHRS-based solutions, extensively described in deliverable D6.4, are also quantified and provided in this document.

4.1 Microgrid embedding shaft generator/motor (PTO/PTI)

PTO/PTI, also called shaft generator/motor, are among the most promising retrofitting solutions conceived for reducing fuel consumption and polluting emissions of ships. PTO/PTI are devised in the framework of the hybrid propulsion paradigm [1], [2], [3], [4], [5].

The main advantages of these retrofitting technologies consist of a more efficient electric power generation on-board due to the higher efficiency of the main engines compared to the auxiliary ones, as well as the associated reduced maintenance costs.

The main motivations leading to the adoption of PTO/PTI technology are the following:

- It diminishes the need to burn extra fuel to power electrical systems through separate diesel gensets;
- Fuel savings is significant, especially when coupled with improved operational flexibility;
- The system can drastically decrease the operating hours of auxiliary generators and their need for maintenance;
- It helps main engines run at a more efficient operating point with lower fuel consumption.

The main benefits can be synthetized as follows:

- Small space requirement;
- Low installation cost;
- Low noise levels;
- High reliability;

On the contrary, the main drawbacks are:

- No electric power generation while in port;
- Increased load on the main engine of the ship;

The mechanical connection of an electrical machine on the shaft of the main engine, typically by dual-in/single-out reduction gearbox, can be exploited to fulfil the tasks described hereinafter.

In *power-take-off (PTO)* generator, commonly known also as a shaft generator, part of the mechanical power from the propulsion engines is transformed into electrical power and transferred into the shipboard power grid by a gearbox and electric generator. Such a configuration reveals, in many situations, the most efficient way to produce the electrical power, instead of running additional engines to produce it (auxiliary generators). For frequency variations and voltage matching, different configurations have been devised. The main advantages of these systems is more efficient electric power generation due to the higher efficiency of the main engines compared to the auxiliary ones,

as well as the associated reduced maintenance costs. Furthermore, through this operation, PTOs can improve the efficiency of the main propulsion engine, as they can shift its operating point closer to its minimum consumption region.

In *Power-take-in (PTI)*, i.e., propulsion electrical motor mode of operation, the shaft generator is operating as a synchronous motor (electrical power being supplied by the vessels auxiliary diesel generator sets). It can either provide a boost in power, working alongside the main engine to increase vessel speed, or it allows the main engine to reduce power, thereby lowering fuel consumption and wear on the main engine. It can be exploited for electrical propulsion for several options of utilization.

Electrical mode is typically adopted at a lower power range, during operations such as sailing out from harbour or running the vessel in emission-free sea areas where specific restrictions are valid (if energy storage are exploited as source of energy). Hybrid mode is typically adopted either to improve propulsion engine performance or to boost maximum speed/thrust out of the propulsion drive train. This mode reveals a very interesting option, also in terms of vessel design, whereas operation profile contains short time intervals of required full power, like pushers, harbour tugs often do, or in case small propulsion engine. A further operation mode, typically adopted in case of an absence of the main engine for increasing the redundancy of the propulsion system, is the so-called power-take-home (PTH). Unlike the PTI mode, in PTH operation, the shaft generator requires a self-starting capability to run up as a motor from zero speed.

Recently, discussions regarding underwater noise have been ongoing. By applying a battery pack to propel the vessel in PTH mode, it is possible to stop the genset and thereby mitigate the underwater sound radiation from energy production on the vessel. As an alternative, battery propulsion utilising electrical energy from gensets suspended on elastic chocks to drive a shaft motor in PTH mode will also greatly reduce underwater noise emissions. Some ports reduce fees for vessels equipped with special underwater noise reduction devices.

As in [6], when a vessel manoeuvres at low rpm, such as at port, the PTO feature is not engaged. Instead, a genset covers the hotel load. When the vessel has left the port and gained speed at open sea, the power delivered by the genset is provided by the PTO and the genset is stopped. At lower rpm, there is a smaller margin to the torque limiter.

This margin narrows when using the PTO, which means a reduction of the acceleration power of the vessel. The consequence is that the time period in which the vessel remains within the barred speed range increases. This is undesirable due to the torsional vibrations in the ME shaft. The vast majority of vessels with PTO are not equipped with a propeller shaft clutch (PSC), which is only installed if power taker home (PTH) is desired.

The main configurations for integrating PTO/PTI technologies on board of ships are the following:

- PTO/gear constant ratio (PTO-GCR)
- PTO/constant frequency mechanical (PTO/CFM)
- PTO/constant frequency electrical (PTO-CFE)
    - PTO-CFE with high speed generator (gear-box)
    - PTO-CFE with low speed generator (direct drive)

An extensive analysis of the above cited configurations has been reported in Deliverable "*D6.4 - Investigation of Retrofitting Options on Ship Electrification Plant*", where the pros and cons of each solution have been properly cited. Therefore, further details have been omitted in this document.

Based on the requirements chosen by the shipowner of the M/V Kastor ship, as written in Deliverable D6.2, the low-speed generator PTO/CFE configuration has been chosen, since it permits the highest controllability and flexibility for the use of the shaft generator as well as the highest capability to minimize the fuel consumptions and polluting emissions. For this reason, only the chosen configuration will be considered in the following. The PTO/CFE technology is supposed to be mechanically connected to the MAN B&W S60ME-C8.5-TII engine [7]

Figure 1 shows the block diagram of the chosen low speed PTO/CFE configuration. It can be clearly observed that to decouple the main engine mechanical speed from the frequency of the shaft generator, an AC-AC power converter is needed. Such an AC-AC converter usually comprises of two voltage source inverters (VSI) in a back-to-back configuration to guarantee a full bidirectional power flow between the electrical machine and the on-board micro-grid. A typical configuration of the two VSI in back-to-back configuration is shown in Figure 2.

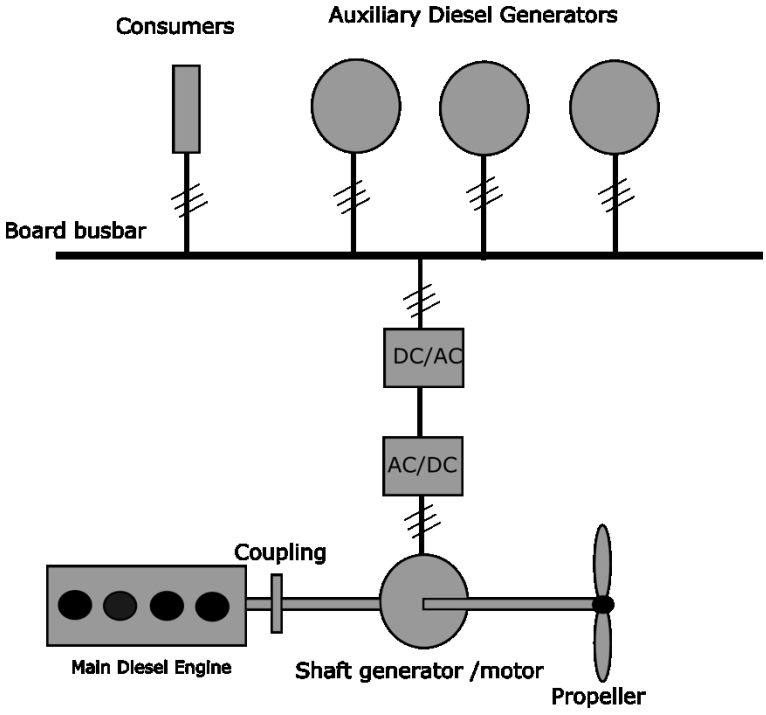

Figure 2: Typical PTO schemes; PTO-CFE system with low speed generator.

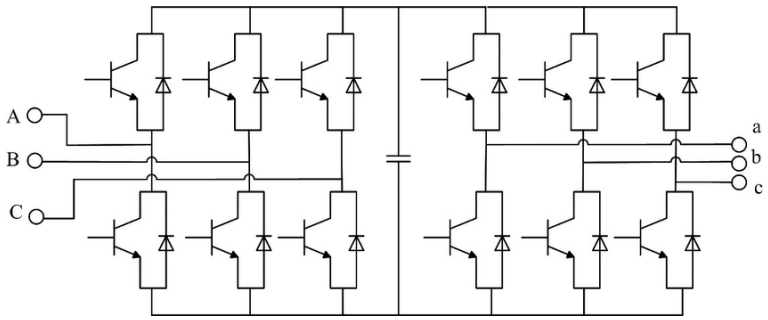

Figure 3: VSIs in back-to-back configuration.

4.1.1 Design of the PTO/PTI for the ship under study

As in [8], the shaft generator reduces EEDI and assists in reaching EEDI compliance. Compared to other means of increasing the efficiency of the total machinery plant on board, a shaft generator is often the most reliable and cheapest solution. Regardless of whether the electric power output of the shaft generator must be dimensioned to cover the total electric load while sailing, or the electric load for 80% of the operating time, as an example, or operate in parallel with the gensets during peak load, an optimization exercise that largely depends on the vessel type and intended trade is done. When evaluating the benefits of a shaft generator, the increased SFOC (Specific Fuel Oil Consumption) resulting from the increased load on the ME must be considered.

Dimensioning the optimum capacity of a PTO is a multi-disciplinary design exercise, where not only the need for electric energy on board the vessel in various conditions is to be considered, but the possibilities for a PTO to work within the ME load diagram, while maintaining a stable speed in presence of the PTO is essential.

In the following, two design methodologies will be shown. Each of them has been conceived considering the load limits of the MAN B&W S60ME-C8.5-TII engine. In particular, the following limits have been considered:

- PTO layout limit, which sets the limit for the combined engine load for propulsion and PTO
- Design limits set to ensure rpm stability.

The load diagram of the MAN B&W engine defines the power and speed limits relative to the specific maximum continuous rating (SMCR) point, specified within the engine layout diagram. The position of the SMCR point within the layout diagram does not influence the appearance of the load diagram. Figure 4 shows the load diagram of a MAN B&W engine, where speed and power are expressed as a percentage of their rated values.

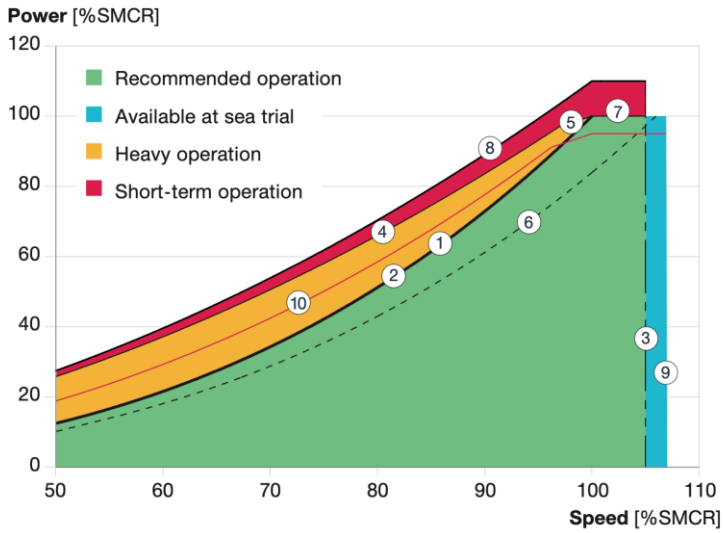

Figure 4: Typical load diagram of a MAN B&W engine.

Figure 4 shows the presence of some working regions and lines. In particular:

Line 1: The engine layout curve, which passes to the 100% SMCR rpm and the 100% SMCR power point. The curve coincides with curve 2.

Line 2: The heavy propeller curve is the light propeller curve (line 6) shifted to the left by the propeller light running margin (LRM) of the propeller. The LRM is included to account for added resistance from wind, waves and hull fouling.

Line 3: Maximum continuous rpm. For engines with SMCR on the L1-L2 line in the layout diagram, up to 105% of L1-rpm can be utilised.

Line 4: This line represents the torque/speed limit for continuous operation of the engine, which is mainly defined by the thermal load of the engine components.

Line 5: The line represents the maximum mean effective pressure (mep) acceptable for continuous operation.

Line 6: The light propeller curve for a clean hull and calm weather. This curve is often used for propeller layout.

Line 7: Maximum power for continuous operation. When increasing the rpm towards lines 3 and 9, the maximum power for continuous operation cannot exceed 100%.

Line 8: Normal overload operating limit of an engine without the AWC functionality.

Line 9: This is the maximum acceptable engine rpm at sea trial. 110% of SMCR-rpm, but no more than 107% of L1-rpm if permitted by torsional vibrations.

Line 10: This is the PTO layout limit explained in the following.

According to the above defined lines, some working regions are defined, marked by different colors. The recommended working region is indicated in green, the heavy operation region in yellow, the short-term operation in red and finally, the sea trial region in blue.

To find the PTO layout limit, the following considerations should be made.

When adding a PTO to the ME, the torque required for the PTO is added on top of the torque required for driving the propeller at the set speed. As a result, the operating point in the engine load diagram moves upward towards the torque limit of the engine.

When dimensioning a PTO, it is important to ensure a stable PTO operation by considering the resulting increase of the torque required, and the resulting engine load. It is mainly done by balancing the thermal loads on the engine, and by ensuring an operating margin for torque variations resulting from, for example, added wave resistance. In order to balance these considerations in the dimensioning of the PTO design capacity, a PTO layout limit has been established.

Table 4 gives the PTO mechanical power allowed under the PTO layout limit in relative figures. The mechanical power of a PTO is the difference in power between the light propeller curve (line 6) and the PTO layout limit (line 10), see the following equation.

$$P_{PTO} = P_{SMCR}\left[P_{PTOlimit} - \left(\frac{n}{1+LRM\%\, n_{SMCR}}\right)^3\right] \quad (1)$$

Here P_{SMCR} and n_{SMCR} are the power and the engine speed at the SMCR point respectively, n is the specific engine speed at which the mechanical PTO power is generated, and LRM is the light running margin. The magnitude of the propeller LRM influences the power available for PTO and thus constitutes a criterion for its design.

It should be noted that, for the Kastor ship, the PTO/PTI system is supposed to be activated only for speeds of the main engine above 50% of n_{SMCR} =45 rpm.

Table 4: SMCR dependent values for the mechanical power allowed under the PTO layout limit given in relative figures.

RPM [% SMCR]	$PTO_{layout\ limit}$ [% SMCR]
60 − 96.2	100 × (rel. rpm [%] / 100%)$^{2.4}$
96.2 − 100	95 × (rel. rpm [%] / 100%)
>100	95

Design method 1

The first design method of the PTO/PTI specifically for the Kastor ship is based on the electrical load analysis. In practice, it is supposed that during PTO operation, it can cover the overall demand of the electrical load power, while respecting the PTO load limits of the MAN B&W S60ME-C8.5-TII engine, as explained above.

The nominal curve of the MAN B&W S60ME-C8.5-TII engine is the following:

$$P_1(n) = c_1 \cdot n^3 = 0{,}13441 \cdot n^3 \quad (2)$$

where $c_1 = \frac{P_{SMCR}}{n_{SMCR}^3} = \frac{9930}{90{,}4^3} = 0.013441$

In this case, the light running margin has been assumed to be equal to 8 %.

The light running power curve can thus be written as:

$$P_{LRM}(n) = c_{LRM} \cdot n^3 => P_{LRM}(n) = 0{,}01245 \cdot n^3 \quad (3)$$

Where $c_{LR} = \frac{P_{SMCR}}{((1+LRM)\cdot n_{SMCR})^3} = \frac{9930}{(1+8\%)\cdot 90{,}4^3} = 0{,}0124$

As for the PTO limit power, it can be written as:

$$P_{PTOlimit} = P_{SMCR} \cdot \left(\frac{n}{n_{SMCR}}\right)^{2.4}, \; for\; n \in 50\%\; to\; 96.2\%\; of\; SMCR \quad (4)$$

Figure 5 shows the main engine nominal curve, power vs speed, the engine load diagram, the light running margin curve and finally the PTO limit power. It can be observed that the PTO layout limit curve is within the Load Diagram limit curves, which is to be expected and fully acceptable. The amount of available power for PTO usage is given by the difference between the PTO Layout limit curve and the LR curve.

Figure 6 shows the table of the electrical load of the Kastor ship, divided in terms of continuous load, intermittent load, and total required power.

It can be noted that the total required power is 521,2 W. Assuming average efficiencies of the inverter and rectifier to be equal to 0.985 and 0,975 respectively, the electrical power required by the PTO generator to cover the overall demand of the load would be:

$$P_{e,input} = \frac{P_{e.output}}{n_{grid} \cdot n_{rectifier} \cdot n_{inverter}} = \frac{521}{0.99 \cdot 0.975 \cdot 0.985} = 548kW \quad (5)$$

For the vessel under study, a PTO system can cover only the power demand of the normal sea service without ballast water exchange and EGCS.

Looking at Figure 5, it can be noted that, at the working speed of the ME equal to 45 rpm, as well as for higher speeds, the difference between the light running margin curve and the PTO limit curve is higher than 548 kW, which is the electrical load. It perfectly ensures the stability of the engine PTO system in the whole working range of the PTO.

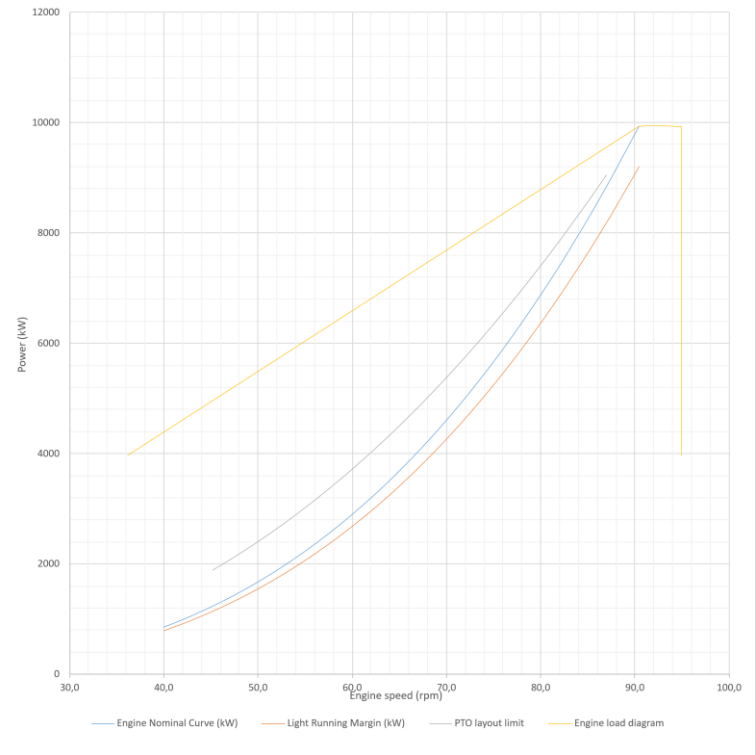

Figure 5: MAN B&W S60ME-C8.5-TII nominal curve, load diagram, light running margin curve and the PTO limit power.

ELECTRIC POWER BALANCE																				SC4669(PZ-2)-601-01JS								PAGE 9
		load		Normal sea service				At port (In/Out)				At Loading/unloading				Harbour Service				Emergency Service				Remark
No.	Consumer	P	Set	Load	Use	C.L.	I.L.	Load	Use	C.L.	I.L.	Load	Use	C.L.	I.L.	Load	Use	C.L.	I.L.	Load	Use	C.L.	I.L.	
		kW		Factor	Set	kW	kW	Factor	Set	kW	kW	Factor	Set	kW	kW	Factor	Set	kW	kW	Factor	Set	kW	kW	
	CONTINUOUS LOAD					472.3				1034.5				276.1				240.2				72.6		
	INTERMITTENT LOAD						122.3				201.2				336.3				291.9					
	INTERMITTENT LOAD DIVERSITY FACTOR						0.4				0.4				0.4				0.4					
	INTERMITTENT LOAD REQUIRED POWER						48.9				80.5				134.5				116.8					
	TOTAL REQUIRED POWER (kW)					521.2				881.2				410.6				357.0				72.6		
	BALLAST WATER EXCHANG AND EGCS					1097.2				1189.4				948.6										
RUNNING GENERATORS CONDITION																								
1	RUNNING GENERATORS (kW x SET)			720x1				720x2				720 x 1				720x1				120X1				
	STANDBY GENERATORS (kW x SET)			720X2				720x1				720x2				720x2				0				
	LOAD FACTOR (%)			72.40%				61.19%				57.03%				49.58%				60.53%				
2	RUNNING GENERATORS (kW x SET)			720x2				720x2				720x2												
	STANDBY GENERATORS (kW x SET)			720x1				720x1				720x1												
	LOAD FACTOR (%)			76.20%				82.60%				66%												
	NOTES :																							
1	C.L. : CONTINUOUS LOAD																							
	I.L. : INTERMITTENT LOAD																							
2	*BALLAST EXCHANGE AT SEA , CARGO HOLDING & ARRIVAL OR DEPARTURE																							
3	CONDITION 1:WITHOUT BALLAST , SCRUBBER SYSTEM at VGP OPERATION (SULPHUR REDUCTION 3.5% to 0.1%)																							
	CONDITION 2:WITH BALLAST,SCRUBBER SYSTEM at VGP OPERATION (SULPHUR REDUCTION 3.5% to 0.1%)																							

Figure 6: Electric load table of the Kastor ship.

Design method 2

The second design method of the PTO/PTI system is based on the analysis of the experimental data on the Kastor ship provided in the framework of the project. A set of experimental data ranging over

a period of 2 years, provided by the ship owner for the disposal of the project, has been analyzed in the Matlab environment.

A preliminary design of the PTO/PTI system has been made with the aim of minimizing the main engine specific fuel oil consumption (SFOC). The design has been made under the assumption that the speed mission profile of the ship (rotating speed of the ME), in the presence of the PTO/PTI system, is not modified with respect to the case of absence of it. This is a reasonable assumption.

Figure 7 shows the nominal propeller power curve, the light running propeller curve and experimental data (only for positive powers).

It can be easily observed from the experimental data that the main engine power is, for each value of the ME speed, above the rated power curve and far above the light propeller curve. It means that in a real-world scenario the propeller is frequently loaded over the rated power.

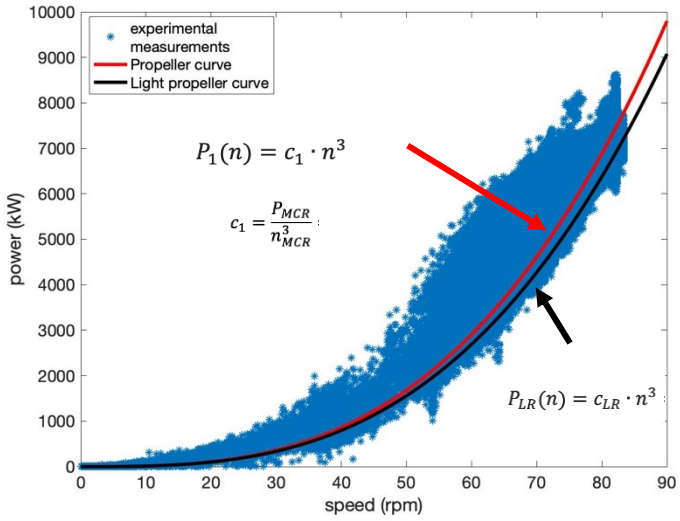

Figure 7: Propeller curve, light run propeller curve and experimental data.

As recalled above, the PTO/PTI system is supposed to be activated only at main engine speeds above 50% n_{MCR} (45 rpm). Experimental measurements on Kastor ship show that the main engine speed is below 45 rpm for 47% of the overall mission time, with 43 % at zero speed. It fully justifies the potential adoption of PTO/PTI system from the point of view of the ship mission profile.

Figure 8 shows the specific fuel oil consumption (SFOC) map of the main engine model MAN B&W S60ME-C8.5-TII, as a function of the power and speed of the engine. On the same figure, the instantaneous working point of the engine in a 2-year interval is plotted. Such points have been divided into two clusters, for engine speeds below (red) and above 45 rpm.

Looking at Figure 8, the following considerations could be made. Firstly, the SOFC surface of the MAN B&W S60ME-C8.5-TII engine is almost flat, confirming the good performance of such an engine. In particular, the maximum variation of SOFC is almost 15 g/KWh over a peak of SFOC equal to 185 g/KWh. It implies that there exist very limited degrees of freedom to reduce or minimize the fuel consumption action of the PTO. Moreover, the working points for speeds below 45 rpm are limited, and are concentrated in the low power / medium speed region.

Figure 9 shows the power versus speed curve corresponding to the minimum SFOC for each engine speed, obtained from the SFOC surface in Figure 8, as well as the engine experimental working points. Operating points show that the main engine is not always operating at a minimum SFOC, as expected. It implies that PTO/PTI can be designed so to make the main engine work at its minimum SFOC for each rotating speed.

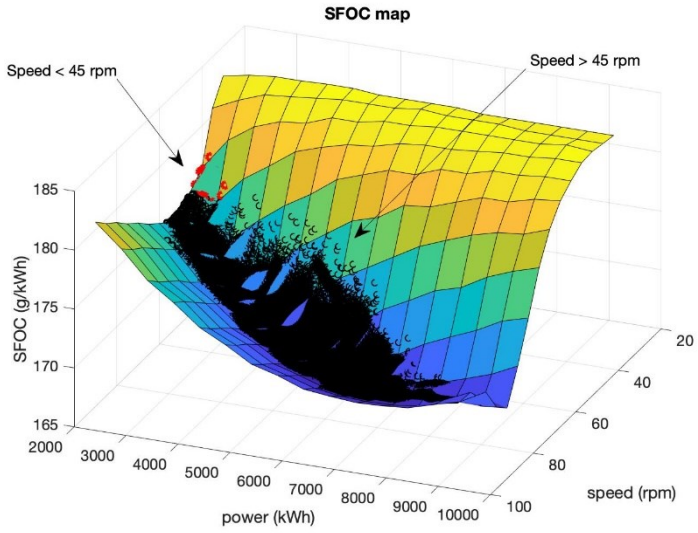

Figure 8: SFOC of the MAN B&W S60ME-C8.5-TII, as a function of the engine power & speed.

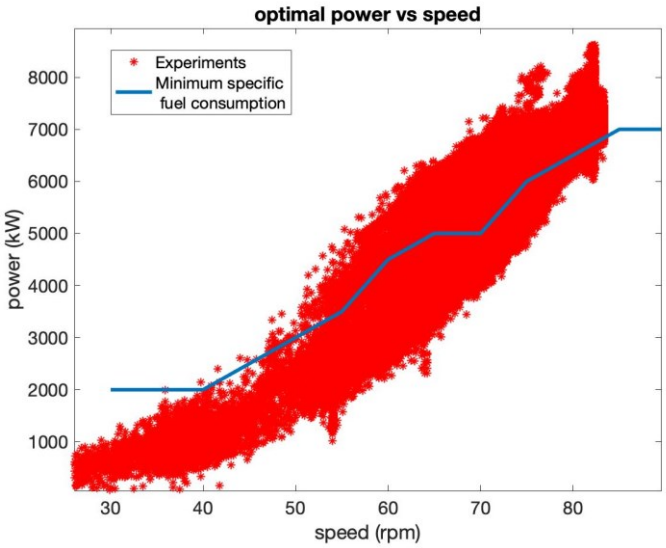

Figure 9: Minimum SFOC power versus speed curve.

In order to design the PTO/PTI system, only the experimental data corresponding to the engine speed above 45 rpm have been considered. The difference ΔP between the minimum fuel consumption main engine power and the real measured main engine power has been computed for each working point. Figure 10 shows the ΔP experimental points versus the engine speed. The same figure also shows the PTO limit curve defined as:

$$PTO_{layout\ limit} = \begin{cases} P_{SMCR} \cdot \left(\frac{n}{n_{SMCR}}\right)^{2.4}, for\ n \in 50\%\ to\ 96.2\%\ of\ SMCR \\ P_{SMCR} \cdot 0.95 \cdot \left(\frac{n}{n_{SMCR}}\right), for\ n \in 96.2\%\ to\ 100\%\ of\ SMCR \\ P_{SMCR} \cdot 0.95, for\ n > 100\%\ of\ SMCR \end{cases} \quad (6)$$

It can be seen that all experimental points lie below the PTO limit curve, confirming that a properly designed PTO is able to guarantee that the main engine works at its minimum SFOC in every working condition, still guaranteeing the stability of the system (a sufficiently high margin with respect to the PTO limit curve). The figure also shows that, to guarantee the main engine work at its minimum SFOC, the electrical machine of the PTO/PTI system is required to work sometimes as a generator and sometimes as a motor.

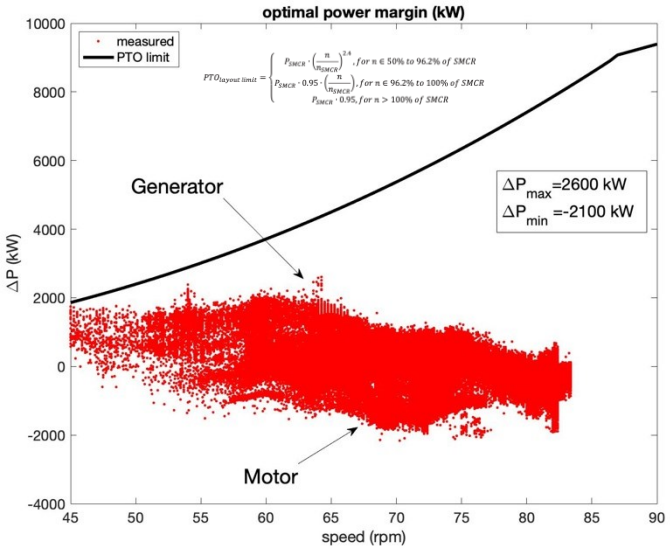

Figure 10: ΔP experimental points versus the engine speed.

Analyzing Figure 10, it can be deduced that the ΔP_{max} = 2600 kW and ΔP_{min} = -2100 kW, implying that the design can be performed assuming the most demanding configuration consisting of the generator. Ref. [6] suggests considering an efficiency of the PTO in the range of 90-95%. Assuming the lowest value of 90%, the design power of the shaft generator should be 2800 kW. A generator of such a rated power would guarantee that the main engine always works at its minimum SFOC, still guaranteeing the electric load of the ship to be properly covered only by the shaft generator.

It should be however noted that, looking at Figure 6, the maximum required power by the load is 521,2 W. It implies that the shaft generator would be over dimensioned with respect to the load of a factor 5.5, with consequent increase of cost, weight and dimensions. Moreover, the system would almost always work without optimizing the SFOC, since the generated power could not be used by the load. Moreover, conceiving the presence of a storage system able to store the extra power generated by the PTO would not be sensible, since its rated power and energy would be too big.

A deeper insight into the experimental data has further shown that, reducing the rated power of the shaft generator from 2800 kW to 1000 kW, would imply that the main engine is able to work at its minimum SFOC for 90 % of the working conditions, adopting a generator of rated power 2/3 smaller.

Assuming this hypothesis, the rated power of the generator would still be higher than the maximum required power by the load, but relatively close to it.

Based on the above considerations, the rated power of the shaft generator has been assumed equal to 1 MW.

4.2 Microgrid embedding integrated PV system

Different operation modes are possible when a PV generator is integrated into a SPS to supply part of the auxiliary power. These modes depend on whether the PV source is operated as stand-alone (also known as off-grid mode) or as grid-connected. Each of such configurations has pros and cons. Particularly, the off-grid mode is characterized by simplicity, not involving any synchronization issue with the on-board AC grid; at the same time, it requires large ESSs to ensure the continuity of electricity supply to the loads connected to the PV source. On the other hand, in the grid-connected mode, it will be possible to reduce the size of the storage, but a proper control design is required to ensure that the PV output conforms in voltage, frequency and phase to the electrical characteristics of the SPS. Hybrid configurations have been also proposed to overcome limitations of the previous schemes [5].

Additional studies needed for realizing effective PV integration and operation in SPS include power quality aspects, as well as interactions of PV systems with protection coordination, especially considering the low electrical inertia of SPSs. PV integration in shipboard DC distribution systems with related stability issues and system-level management of shipboard hybrid generation systems involving PV (e.g., economic dispatch of PV-ESS systems), also deserve investigation [9]. However, these aspects go beyond the scope of this project.

4.2.1 Off-grid PV plant

Off-grid photovoltaic (PV) systems are solar power systems that operate independently of the traditional electrical grid. These systems harness sunlight through solar panels to generate electricity, which is then stored in batteries for later use. Off-grid PV systems are ideal for locations where access to the central power grid is unavailable, unreliable, or too costly to extend. They provide a sustainable, self-sufficient energy solution, reducing dependence on fossil fuels and enhancing energy security. These systems are commonly used in rural areas, remote homes, cabins, or mobile setups like boats and recreational vehicles. With advancements in solar technology, off-grid PV systems are becoming more efficient, affordable, and accessible, making them an attractive option for both residential and commercial applications.

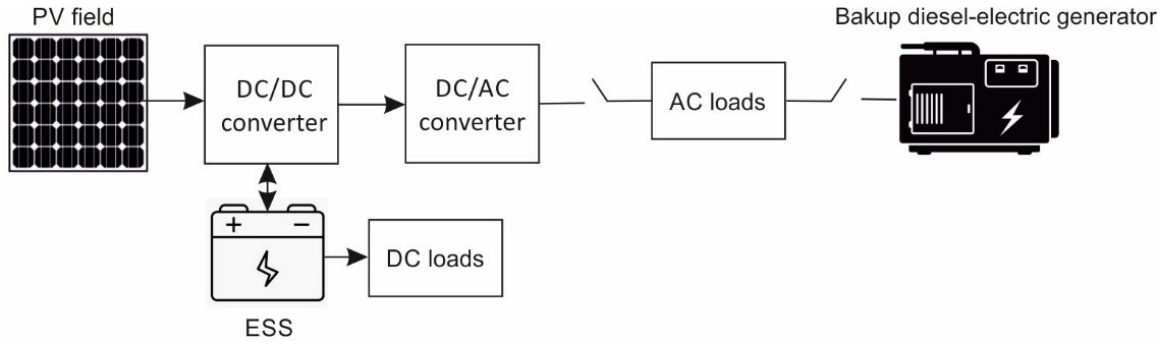

Figure 11: Off-grid schematic representation of a shipboard PV plant.

Figure 11 shows the schematic outline of an off-grid shipboard PV plant.

The battery sizing of an off-grid PV system is generally done by making sure that the battery can provide sufficient reserve during cloudy days or periods of high usage. Most land-based off-grid PV systems aim for 2-3 days of self-sufficiency. In this case study, where the peak power of the PV plant is about 400kW, and the PV panels are exposed to 3 peak hours on average it is found that a daily energy of 400 x 2.5 = 1,000 kWh will be supplied to the load. In such a situation, the battery size of a Li-ion battery needed to ensure two days of self-sufficiency with a depth of discharge (DoD) set to 80% can be obtained as: (1,000 x 2)/0.8 = 2,500 kWh.

Maximum powers needed during battery charge/discharge should also be evaluated to identify the corresponding requirements for the battery. These power requirements can be deduced by the analysis of the PV system's load profile. It is obvious that the introduction of a backup storage system onboard for an off-grid photovoltaic system results in an increase in the ship's technical weight and volume, as well as additional costs, whose assessment goes beyond the scope of this report.

As far as the power converters are concerned, the following considerations apply.

The DC/DC bidirectional converter interfacing the battery (ESS) with the PV plant (charge controller) must be selected so that its current rating matches the output of the solar array. This ensures safe charging of the battery bank. Maximum Power Point Tracking (MPPT) controllers should be used within such a converter for helping optimization of power extraction from the PV panels, especially in low-light conditions.

The DC/AC converter (inverter) must be able to handle the peak load (maximum wattage drawn at any given moment) and with an adequate surge capacity to support devices that require higher startup power. Off-grid inverters should be durable and designed to manage fluctuating load demands effectively.

4.2.2 Grid connected PV plant

Grid-connected photovoltaic plants used in land-based applications are large-scale solar power systems designed to generate electricity and feed it directly into the electrical grid. Unlike off-grid systems, which operate independently, grid-connected PV plants work in tandem with the public utility grid, enabling them to supply power to homes, businesses, and industries. These systems consist of arrays of solar panels that capture sunlight and convert it into electricity, which is then distributed through the grid. Grid-connected PV plants play a key role in the transition to renewable energy, offering a sustainable alternative to conventional fossil fuel-based power generation. They help reduce greenhouse gas emissions, lower electricity costs, and improve grid stability by providing a clean and abundant source of energy.

The concept of a shipboard grid-connected photovoltaic generation system mirrors that of a land-based grid-connected PV plant. In such a configuration the PV panels are connected in parallel to the main busbars, delivering electrical power alongside the diesel-electric generators.

Figure 12 shows the schematic outline of a grid-connected shipboard PV plant.

The presence of an ESS (usually a battery), in this case, is no longer essential, although it may be advisable to include one to ensure stable operation of the onboard electrical grid. As a matter of fact, due to variations in solar irradiation and surface temperatures, especially during a long-term voyage, the output power from the PV system is unstable and intermittent.

According to the IEEE guide for ship power grids [10], the power injected from a hybrid PV system must remain smooth and constant. To maintain a stable power injection, instantaneous fluctuations in PV power should be compensated by the ESS [11]. Furthermore, since SPS is a self-contained isolated micro-grid, the marine diesel generators should be sized for the total power, even with the addition of the PV system.

As for the battery sizing in a grid-connected shipboard PV system, the following considerations apply.

A PV system is a non-inertial power generation system, therefore, when the output power of the PV system suddenly drops due to clouds or object shadows, the battery is discharged to smooth out grid-connected power fluctuations. When the shadows of clouds or other objects move away from the PV modules, the system's power increases rapidly, and the battery is charged with the excess power. To prevent the PV system from causing significant power fluctuations on the ship's power grid, the ship classification societies have imposed limits on the rate of power change. In this kind of power system, the maximum rate of change in grid-connected power (ΔP) cannot exceed 10 kW/min. On such a basis, when the PV output power suddenly decreases from its rated value $P_{PV\text{-}rated}$ to 0 kW, the discharge duration (T) of the battery is $P_{PV\text{-}rated}$ /ΔP. In this process, P_{PV} (t) = $P_{PV\text{-}rated}$ – ΔPt; therefore, the rated capacity of the battery $E_{b\text{-}rated}$ can be obtained as:

$$E_{b-rated} = \int_0^T \frac{P_{PV}(t)}{\eta_{ch} \cdot DoD} dt = \frac{1}{2} T \frac{P_{PV-rated}}{\eta_{ch} \cdot DoD} = \frac{1}{2} \frac{P_{PV-rated}}{\Delta P} \frac{P_{PV-rated}}{\eta_{ch} \cdot DoD} \quad (7)$$

where the term η_{ch} is the charge efficiency of the battery and DoD is the depth of discharge.

In a case like that under study, with a peak power of the PV plant of about 400kW and considering the installation of a Li-ion battery with a charge (discharge) efficiency of 98% and a DoD of 80% the battery rated capacity would be equal to 340 kWh. The electrical configuration is defined based on the grid voltage and the specific technical feature of the chosen battery.

It should be observed that, to effectively respond to power fluctuations from the PV system, the ESS must have sufficient margin to compensate for any power surges. Therefore, the energy stored in the ESS at any given time must meet the following formula:

$$E_b = \int_0^t \frac{P_{PV}(t)}{\eta_{ch} \cdot DoD} dt = \frac{1}{2} t \frac{P_{PV}(t)}{\eta_{ch} \cdot DoD} = \frac{1}{2} \frac{P_{PV}(t)}{\Delta P} \frac{P_{PV}(t)}{\eta_{ch} \cdot DoD} = E_{b-rated} \left(\frac{P_{PV}(t)}{P_{PV-rated}} \right)^2 \quad (8)$$

As far as the power converters are concerned, the following considerations apply.

The ensemble of the DC/DC converter and DC/AC converter interfacing with the PV panels with the power grid is usually referred to as PV inverter. This equipment is devoted to several vital functions such as: DC link voltage control, grid synchronization, current control, MPPT, anti-islanding protection and grid/PV system monitoring. In terms of the required specifications for PV inverters, several key factors need to be considered. First and foremost, high efficiency is essential to ensure optimal performance and minimize energy losses. Alongside this, accurate MPPT is crucial to make sure that the system can operate at its most efficient point, adjusting as conditions change. Another important aspect is compliance with both current and evolving regulations, which ensures that the system remains legally and technically up to date. Monitoring and synchronization with the power grid are also critical for maintaining smooth integration and ensuring that the converter operates flawlessly with the shipboard power grid. Additionally, safety features such as anti-islanding protections are necessary to prevent issues in the event of grid disturbances.

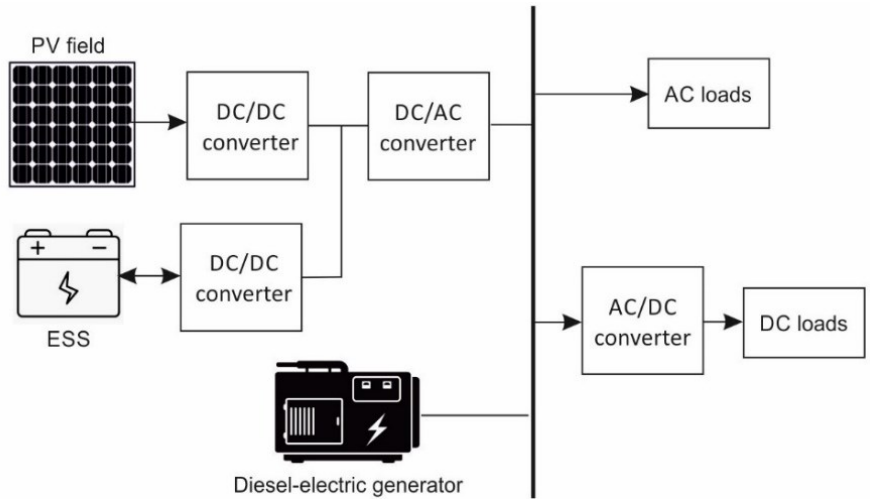

Figure 12: Grid-connected schematic representation of a shipboard PV plant

Furthermore, considerations around isolation, leakage current, and direct current monitoring are important for safeguarding both equipment and users. Finally, maintaining high power quality throughout is essential to prevent disruptions and ensure reliable operation.

The DC/DC bidirectional converter interfacing the battery (ESS) with the PV plant should be finally sized coherently with the power rating of the battery.

Technical literature also exhibits examples of shipboard PV systems which can operate both as off-grid and grid connected thanks to special set up allowing for switching form one configuration to the other [12].

The forthcoming analysis, aimed at determining the energy performance of the PV generation on the ship in the case study, will refer to the case of a PV system connected to the grid without the addition of the storage system.

4.3 Microgrid embedding FC/battery/WHRS

The ship electrification system integrates FCs, batteries, and a waste heat recovery system (WHRS) to DEs to improve energy efficiency, reduce emissions, and enhance operational flexibility. Among the fuel cells evaluated, Phosphoric Acid Fuel Cells (PAFCs) use LNG with onboard reforming for hydrogen production, while Proton Exchange Membrane Fuel Cells (PEMFCs) and Solid Oxide Fuel Cells (SOFCs) operate using externally supplied green hydrogen. PAFCs are mature but less efficient, whereas PEMFCs and SOFCs offer higher efficiencies and lower emissions. Each type was sized and modelled according to ship power demands and space constraints.

Lithium-ion batteries were implemented to support the FCs and serve as a backup during high demand or transient conditions. Battery packs were assembled based on a 440V grid using individual cells and managed through a Constant Current-Constant Voltage charging protocol. Their performance and degradation were simulated using manufacturer data on state of charge (SoC) and state of health. An energy management strategy maintained the SoC between 20% and 80% to extend battery life. Battery output was integrated into the ship's AC system via high-efficiency inverters, enabling smooth operation within the hybrid power architecture.

The WHRS captured exhaust heat from the main engines using an organic Rankine cycle, converting it into additional electrical power. Using engine exhaust gases as a thermal source and R1336mzz(Z) as the working fluid, the system achieved an efficiency of 13.2%, contributing to reduced fuel consumption and emissions. The power contribution from WHRS was factored into the overall system operation to reduce dependency on diesel generators.

An algorithm governed the real-time operation of the electrification system, prioritizing energy sources based on demand and availability. It dynamically allocated load among FCs, batteries, WHRS, and DEs. Each hybrid configuration included at least one DE as a backup, ensuring reliability. Depending on the setup, some configurations were capable of fully replacing two diesel generators, while others matched the output of one. Each component was sized and managed based on performance simulations, environmental impact, and spatial constraints. Together, these technologies formed a hybrid power system that significantly reduces emissions, improves energy use, and enhances the sustainability of ship operations. The detailed integration process and mathematical background for FC/battery/WHRS hybrid systems are presented in D6.4.

The baseline configuration comprises of three DEs with a total power output of 720 kW. The hybrid configurations are designated as Cases 1 through 4. In Case 1, the system includes two AEs and one SOFC, providing a fuel cell power output of 250 kW, while the battery capacity is 273 kWh. Case 2 features two DEs paired with two PEMFCs, delivering a combined power output of 400 kW and a battery capacity of 123 kWh. In Case 3, the configuration again includes two DEs, coupled with one PAFC, maintaining a power output of 440 kW, with a battery capacity set at 83 kWh. Finally, Case 4 consists of three DEs and excludes any fuel cells, with an increased battery capacity of 600 kWh. All hybrid configurations incorporate a WHRS that achieves a mean power output of 197 kW.

5 Evaluation of efficiency design indexes by introducing novel technologies

The shipping industry has long been focused on improving fuel efficiency. Although ships are globally recognized as the most fuel-efficient mode of bulk transportation, the IMO GHG Studies released in the last decades revealed significant opportunities for further enhancing energy efficiency. These improvements can primarily be achieved using existing technologies, such as more efficient power and propulsion systems, advanced hull designs, and the construction of larger vessels. In other words, technical and design-based measures have the potential to substantially reduce fuel consumption and CO_2 emissions on a per-capacity basis (ton-mile).

The Energy Efficiency Design Index (EEDI) and the Energy Efficiency Existing Ship Index (EEXI) address these technical and design measures by establishing a minimum energy efficiency standard for new ships. This encourages the continuous development of all elements that affect a ship's fuel efficiency while distinguishing between design/technical measures and operational/commercial practices. Such design efficiency indexes are useful since they make it possible to compare the energy efficiency of individual ships, assessing how they perform relative to similar vessels of the same size and transport tasks. On such a basis, the following sections assess the performance of the vessel under study when PTO/PTI and PV generation are introduced as electrification retrofitting measures. The attained EEXI is calculated under different situations (with only PTO/PTI, with only PV and with both PTO/PTI and PV) and compared with the actual attained EEXI of the ship.

For the reader's convenience, the attained EEXI formula with explanation of the meaning of the single terms is shown in Figure 13.

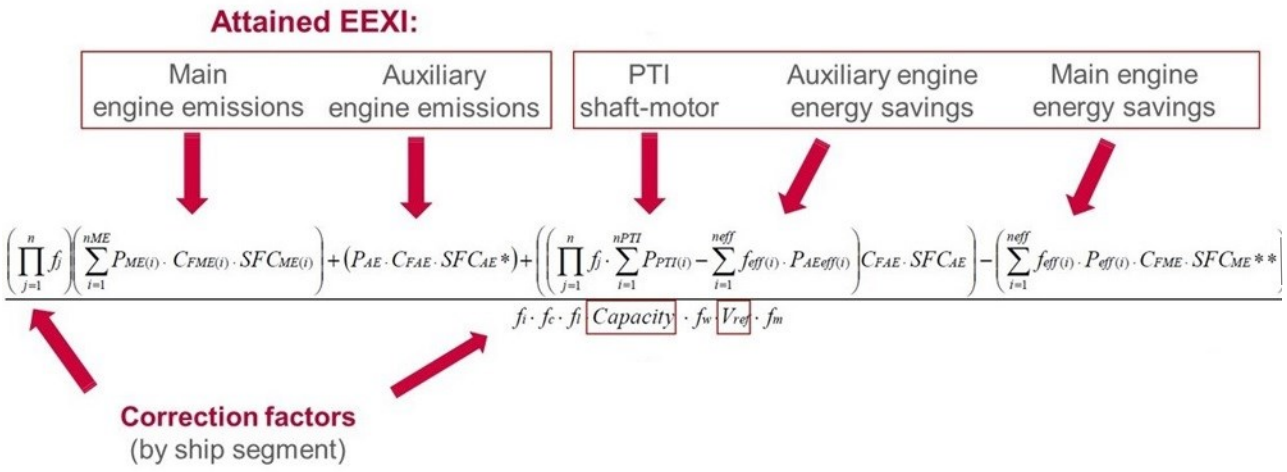

Figure 13: Attained EEXI formula with explanation of its terms.

5.1 PTO/PTI

The Resolution MEPC.308(73) (Adopted On 26 October 2018) – "2018 Guidelines on the method of calculation of the Attained Energy Efficiency Design Index (EEDI) for new Ships" explains the method of computation of the EEXI index if the PTO/PTI technology is integrated [13]. The total shaft power

– at which Vref is measured – is given by the sum of main engine(s) power $\sum_{i=1}^{nME} P_{ME(i)}$ (see paragraph 2.2.5.2, "Option 1") and the PTI power $\sum_{i=1}^{nME} P_{PTI(i),Shaft}$ (see paragraph 2.2.5.3):

$$\sum P = \sum_{i=1}^{nME} P_{ME(i)} + \sum_{i=1}^{nPTI} P_{PTI(i),Shaft} \quad (9)$$

Main engine(s) power

Where the shaft generator is installed, $P_{PTO(i)}$ is 75% of the rated electrical output power of the shaft generator; but if a shaft generator is installed with the steam turbine, the factor of 0.75 must be replaced to 0.83

$$\sum_{i=1}^{nME} P_{ME(i)} = 0.75 \cdot \left(\sum MCR_{ME(i)} - \sum P_{PTO(i)}\right) \quad \text{with} \quad 0.75 \cdot \sum P_{PTO(i)} \leq P_{AE} \quad (10)$$

Where:

$\mathrm{MCR}_{ME(i)}$	is the rated power of each main engine
$P_{PTO(i)}$	$= 0.75 \cdot MCR_{PTO(i)}$ ($\mathrm{MCR}_{PTO(i)}$ is the rated electrical output power of the shaft generator)
P_{AE}	is the auxiliary engine power (see paragraph 2.2.5.6) required to supply normal maximum sea load including necessary power for propulsion machinery/systems and accommodation (i.e.: main engine pumps, navigational systems and equipment and living on board), but excluding the power not for propulsion machinery/systems (i.e.: thrusters, cargo pumps, cargo gear, ballast pumps, maintaining cargo, e.g. reefers and cargo hold fans)

Shaft motor(s) power:

In general

$$\sum_{i=1}^{nPTI} P_{PTI(i),Shaft} = \frac{\sum_{i=1}^{nPTI}\left(0.75 \cdot P_{SM,max(i)} \cdot \eta_{PTI(i)}\right)}{\eta_{\overline{GEN}}} \quad (11)$$

where

$P_{SM,max(i)}$	is the rated power consumption of each shaft motor
$\eta_{\overline{GEN}}$	is the weighted average efficiency of the generator

In the case where shaft motor(s) are installed, $P_{PTI(i)}$ is 75% of the rated power consumption of each shaft motor divided by the weighted average efficiency of the generator(s); but if shaft motor(s) are installed with the steam turbine, the factor of 75% must be replaced to 83%.

$$\sum_{i=1}^{nPTI} P_{PTI(i)} = \frac{\sum_{i=1}^{nPTI}\left(0.75 \cdot P_{SM,max(i)}\right)}{\eta_{\overline{GEN}}} \quad (12)$$

Conclusion

Finally, total shaft power – at which Vref is measured – is given by:

$$\sum P = \sum_{i=1}^{nME} P_{ME(i)} + \sum_{i=1}^{nPTI} P_{PTI(i),Shaft} = 0.75 \cdot \left(\sum MCR_{ME(i)} - \sum P_{PTO(i)}\right) + \frac{\sum_{i=1}^{nPTI}\left(0.75 \cdot P_{SM,max(i)} \cdot \eta_{PTI(i)}\right)}{\eta_{GEN}} \quad (13)$$

Figure 14 shows the attained EEXI calculated for the ship under study, without the integration of any efficiency measure, compared to the baseline EEDI curve (reference) set for bulk carriers by IMO standards according to the following formula:

$$\text{Reference} = \text{a} \times b^{-c} \quad (14)$$

where a=961.79, b=0.477, and c is equal to the DWT of the ship.

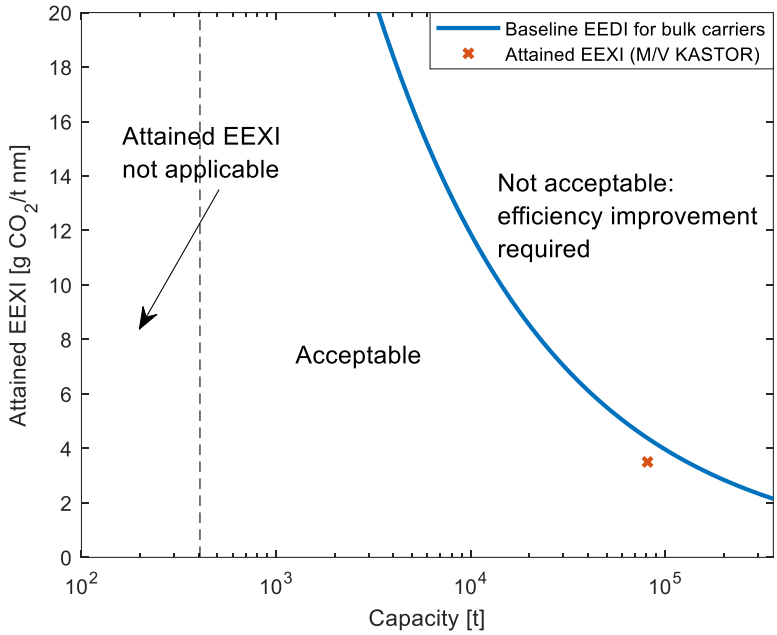

Figure 14: Attained EEXI of the M/V Kastor ship without any efficiency measure.

The new attained EEXI is calculated considering two application cases, i.e., the use of the shaft generator as PTO and the use of shaft generator as PTO/PTI. The obtained values of EEXI were respectively 3.15 g CO_2/t nm and 3.64 g CO_2/t nm. Therefore, considering that the actual declared attained EEXI of the ship is 3.502 g CO_2/t nm, the introduction of the PTO system leads to a reduction in the attained EEXI of 0.352 (-10%), whereas the introduction of a PTO/PTI system implies an increase of EEXI of 0.138 (+3.94%). Figure 15 and Figure 16 show respectively the original attained EEXI compared with the new values obtained with the introduction of PTO and PTO/PTI systems and with the baseline EEDI curve.

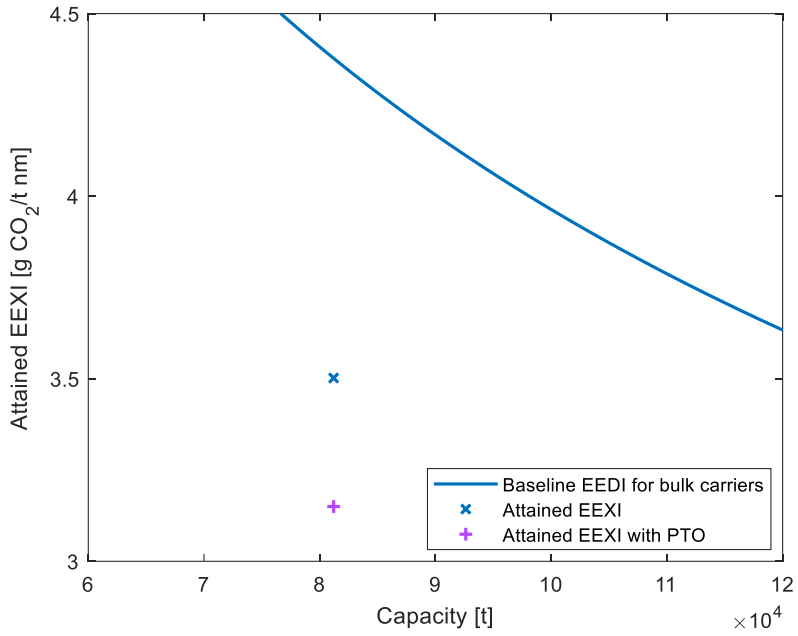

Figure 15: New attained EEXI of the M/V Kastor ship with PTO system.

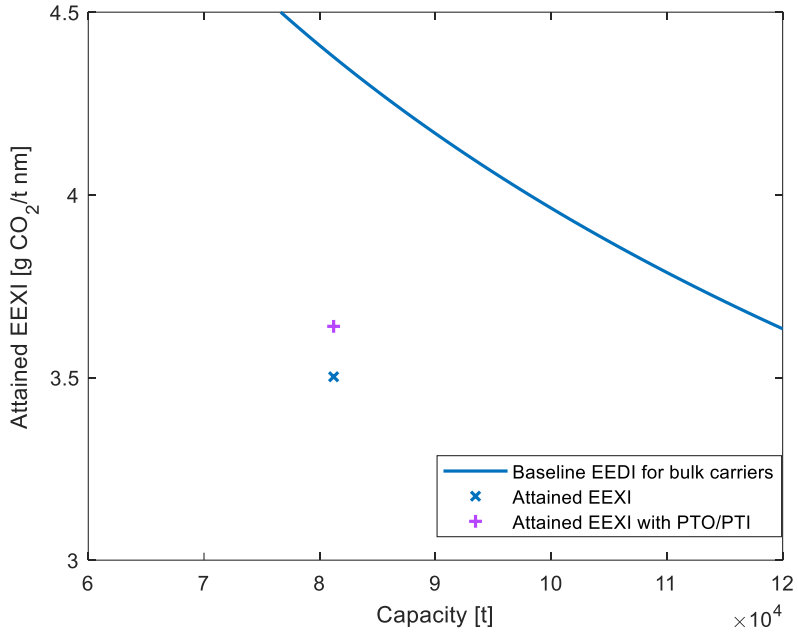

Figure 16: New attained EEXI of the M/V Kastor ship with PTO/PTO system.

5.2 Photovoltaic power generation systems

According to the IMO Resolution MEPC.1/Circ.896 – "Guidance on treatment of innovative energy efficiency technologies for calculation and verification of the attained EEDI and EEXI" The auxiliary power reduction due to the PV power generation system can be calculated as shown in the following equation which expresses the total net electric power (kW) generated by the PV power generation system:

$$f_{eff}P_{AEeff} = \left\{f_{rad}\left(1+\frac{L_{temp}}{100}\right)\right\}\left\{P_{max}\left(1-\frac{L_{others}}{100}\right)\frac{N}{\eta_{GEN}}\right\} \quad (15)$$

The term f_{eff} at first member is the effective coefficient. It can be calculated using the solar irradiance and air temperature of main global shipping routes according to the following equation:

$$f_{eff} = f_{rad}\left(1+\frac{L_{temp}}{100}\right) \quad (16)$$

Here, f_{rad} represents the ratio of the average solar irradiance on main global shipping route to the nominal solar irradiance specified by the manufacturer.

It should be noted that the PV nominal maximum generating power P_{max} is measured under the so-called Standard Test Condition (STC) of IEC standard. STC specified by manufacturer corresponds to the following conditions: Air Mass (AM) 1.5, module's temperature equal to 25°C, and solar irradiance equal to 1000 W/m^2.

The average solar irradiance on the main global shipping route is 200 W/m^2. Therefore, f_{rad} is calculated as follows:

$$f_{rad} = 200\,W/m^2 \div 1{,}000\,W/m^2 = 0.2$$

The term L_{temp} is the correction factor (usually negative) derived from the PV modules' temperature coefficient and expressed in per cent.

The modules' average temperature is estimated to be 40°C, reflecting the typical air temperature along major global shipping routes. Consequently, L_{temp} is calculated using the temperature coefficient f_{temp} (percent/K) provided by the manufacturer, as outlined in the IEC standard 7, with the following formula:

$$L_{temp} = f_{temp} \times (40°C - 25°C) \quad (17)$$

The term P_{AEeff} is the generated PV power divided by the weighted average efficiency of the PV generator(s) under the condition specified by the manufacturer and expressed as follows:

$$P_{AEeff} = P_{max}\left(1-\frac{L_{others}}{100}\right)\frac{N}{\eta_{GEN}} \quad (18)$$

In the above equation η_{GEN} is the weighted average efficiency of the PV generator(s), P_{max} is the nominal maximum generated PV power generation of a module expressed in kW.

The term L_{others} represents the total additional losses, expressed in per cent. These include losses in the power converter, contact losses, electrical resistance, and other factors. Based on experience,

L_{others} is estimated at 10%, with 5% attributed to the power converter and the remaining 5% to other losses. Lastly, N denotes the number of modules used in the PV power generation system [14].

Based on the above-described procedure and on the ship design data provided by Laskaridis (M/ Kastor EEXI technical file), it is possible to estimate the auxiliary power reduction due to the PV power generation system designed in deliverable 6.4 for the ship under study (M/V Kastor), as well as the new attained EEXI.

It is worth recalling that four configurations of PV panel disposition on M/V Kastor ship were explored ("*config_i_j* with *i,j*=1÷2), for each of which four different PV panel models were considered (Premium PS335M-24/T, PANDAYL265C-30b, Solbian SB 47, and Solbian SP 44).

To perform the calculation, information on the auxiliary power reduction due to the PV power generation system, the technical features and number of the different considered PV panels are needed. This information is summarized in Table 5. The remainder of the necessary parameters are deduced by the EEXI documentation of the ship under study.

Table 6 shows the obtained value of $f_{eff}P_{AEeff}$ for each of the considered situations, whereas Table 7Table 7 shows the new values obtained for the attained EEXI once the PV generation system (for any configuration and PV panel model) is introduced. Best and worst cases are highlighted in tables illustrating auxiliary power reduction and the new attained EEXI. For the auxiliary power reduction, it is possible to observe a range of variation from 38.75 kW (worst case) to 107.53 kW (best case).

The analysis conducted in deliverable D6.1 showed that only one of the three diesel electric generating sets is operational during most of the period of operation; it also showed that the load factor of each generator does not exceed 65%. From this information, the auxiliary power reduction, obtained by introducing a PV generation system, ranges from 5% to 15% of the nameplate power of the single diesel electric generator (720 kW); it ranges from 8% to 23% of the electric generator power, considering the electric generator loaded at 65% (468 kW).

Table 5: PV panel technical features and number.

	PV panel model			
	Premium PS335M-24/T	PANDAYL265C-30b	Solbian SB 47	Solbian SP 44
f_{temp} [percent/K]	-0.45	-0.45	-0.27	-0.35
P_{max} [kW]	0.335	0.265	0.164	0.15
N ("config_1_1")	1,404	1,712	3,417	3,664
N ("config_1_2")	741	912	1,938	2,038
N ("config_2_1")	1,313	1,584	3,145	3,384
N ("config_2_2")	637	784	1,683	1,746

Table 6: Obtained auxiliary power reduction due to the PV power generation system.

	$f_{eff}P_{AEeff}$ [kW]			
	PV array configurations			
PV panel model	"config_1_1"	"config_1_2"	"config_2_1"	"config_2_2"
Premium PS335M-24/T	87.7184	46.2958	82.0330	39.7982
PANDAYL265C-30b	84.6113	45.0733	78.2852	**38.7472**
Solbian SB 47	**107.5385**	60.9920	98.9782	52.9667
Solbian SP 44	104.1492	57.9301	96.1902	49.6300

The new attained EEXI ranges from a minimum of 3.4393 (best case) to a maximum of 3.4798 (worst case). Therefore, considering that the actual declared EEXI attained by the ship is 3.502 g CO_2/t nm, the introduction of the PV generation system leads to a reduction in the attained EEXI ranging from 0.022 to 0.063.

Table 7: Attained EEXI by introduction of the PV power generation system.

	Attained EEXI with PV [g CO_2/t nm]			
	PV array configurations			
PV panel model	"config_1_1"	"config_1_2"	"config_2_1"	"config_2_2"
Premium PS335M-24/T	3.4510	3.4754	3.4543	3.4792
PANDAYL265C-30b	3.4528	3.4761	3.4565	**3.4798**
Solbian SB 47	**3.4393**	3.4667	3.4444	3.4714
Solbian SP 44	3.4413	3.4685	3.4460	3.4734

Figure 17 and Figure 18 show the attained EEXI compared with the new values obtained with the introduction of PV generation system in the worst and best cases, respectively.

Although small, the observed EEXI reduction is not to be considered negligible, given that, in the formula for calculating EEXI, the terms relating to auxiliary power are an order of magnitude smaller than the terms relating to propulsion power to which they are added to at the numerator.

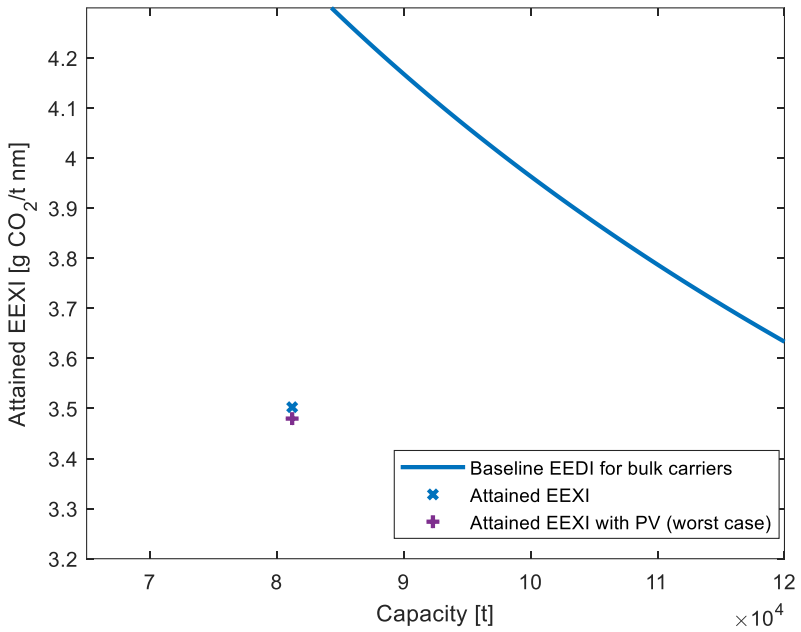

Figure 17: New attained EEXI of the M/V Kastor ship with PV generation system (worst case)

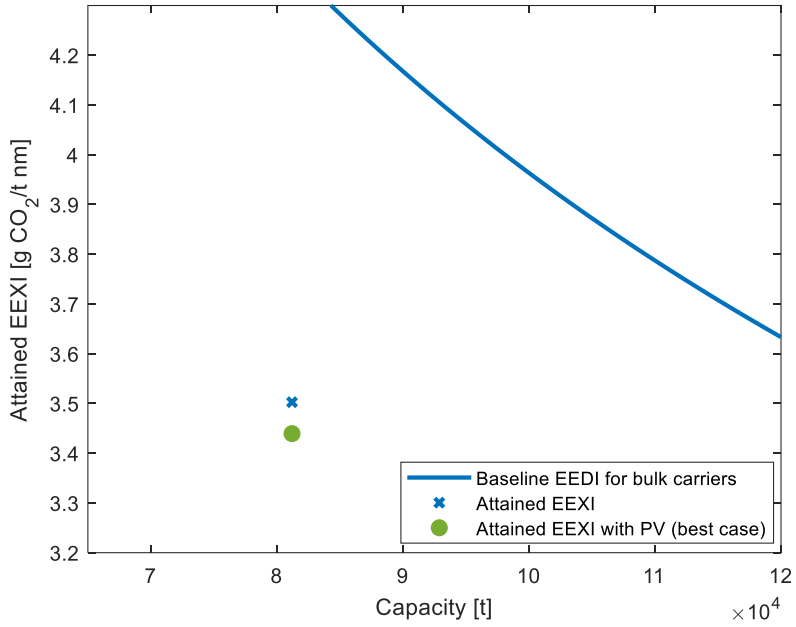

Figure 18: New attained EEXI of the M/V Kastor ship with PV generation system (best case)

6 Analysis of proposed retrofitting solutions based on operational profile of the case study ship

Once the efficiency performance of the considered electrical technologies was verified based on the EEXI design index, the next step was to evaluate the performance of the same electrical technologies based on the operational data of the case study ship (M/V Kastor) provided by Laskaridis. In the following sections the analysis based on operational data of the ship is presented considering, respectively, the use of PTO/PTI and the use of PV generation systems.

6.1 PTO/PTI: Analysis of fuel savings for the main engine and calculation of fuel savings for the diesel engine and emission reduction

Assuming that the rated power of the designed PTO/PTI system is equal to 1 MW (see section 4.1.1), a specific analysis has been carried out on the real operational data of the Kastor ship to quantify the net reduction of fuel consumption as well as polluting emissions in the presence of the shaft generator. As a matter of fact, the presence of the PTO system implies, on one side, an increase in fuel consumption of the ME whose load increases and, from the other side, a decrease of consumption of the diesel engine (DE), whose load decreases. The achievable improvements in terms of fuel consumption and polluting emissions reduction arise from the differences between the SFOCs of the ME and DE. In particular, the fuels typically adopted by the ME and the DE are different. The SFOC of the MGO (Marine Gas Oil), adopted by the main engine, is usually lower than that of the HFO (Heavy Fuel Oil), adopted by the DE. Therefore, adopting the PTO, the instantaneous SFOC of the ME decreases while that of the DE increases.

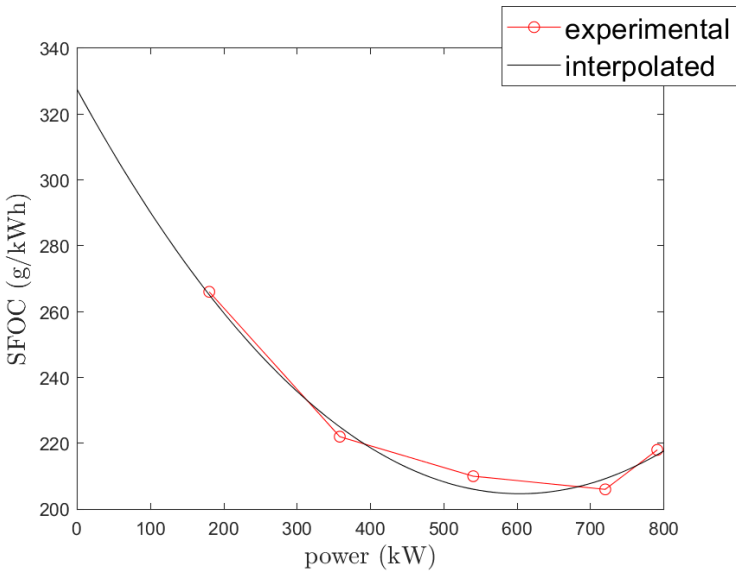

Figure 19: SFOC versus power curve for the Diesel Generator.

As for the Kastor ship under study, the ME SFOC surface has been shown in Figure 8. As for the DE, the SFOC curve has been retrieved exploiting the datasheet of installed DE model YANMAR CO. 6EY22LW, characterized by rated power of 800 kW, rated speed of 720 rpm and rated SFOC at 50% of MCRAE of 215 g/kWh, supplied by HFO. Figure 19 shows the SFOC versus power curve of the DE YANMAR CO. 6EY22LW, depicting the data shown in the datasheet of the manufacturer and the related interpolating second order polynomial curve respectively. A comparison between

Figure 8 and Figure 19 show clearly that the SFOC of the ME is lower than that of the DE for any value of the load power and speed, confirming the possibility to exploit the PTO/PTI technology for reducing the overall fuel consumptions.

The experimental data related to the Kastor ship have been processed assuming that the mission profile of the ship maintains the same. The PTO system has been assumed to work only for engine speed higher than 45 rpm, as required by the ME manufacturer technical manual. For engine speeds lower than 45 rpm, the load power has been assumed to be supplied entirely by the DE. Since the analysis of the experimental data has shown that the overall load power, in these working conditions, is always lower than the rated power of the DE, the load power has been supplied by just one DE, in particular DE1 to optimize the use of the Des.

An easy management system has been adopted to instantaneously decide the power source that supplies the electrical load on-board in any ship working condition. The main target of the management system is to generate electrical power by the PTO, since the SFOC of the ME is lower than that of the DE in all working conditions. It implies that power is generated by DE only if strictly necessary. In the following, P_{PTOopt} is the PTO power permitting the ME work at its minimum SFOC and P_{load} is the instantaneous value of the overall load electrical power. The adopted management system can be described as follows.

- If $P_{PTOopt} < P_{load}$ then the PTO power reference will be set equal to $P_{PTOref}=P_{PTOopt}$, and the remaining part of the load power is supplied by the DE power P_{DE}, $P_{DEref} = P_{load}-P_{PTOopt}$. Within these operating conditions, the ME operation is optimized, while there are no degrees of freedom to optimize the operation of the DE.
- If $P_{PTOopt} > P_{load}$, then the load will be entirely supplied by the PTO, $P_{PTOref}=P_{load}$. The ME operation is not optimized for these working conditions.

All the figures shown in the following compare the experimental results provided by the ship owner in the current working conditions (no retrofitting technologies implemented) with those obtained in the presence of the designed PTO. As for the case of application of the PTO, the analysis has been performed twice, with ideal and real rated powers of the shaft generator, respectively equal to 2,6 MW and 1 MW respectively. This further comparison has been made to show the worsening performance of the PTO, due to its derating with respect to the ideal design. As for the following results, the PTO system has been supposed to be managed as above described. Figure 20 shows the ME power, with and without the PTO, and Figure 21 shows the PTO power in the case of its adoption. It can be observed that the ME power is the lowest in case of not adoption of the PTO, followed by the case of the integration of PTO with rated power of 1 MW and finally by the case of its integration with rated power of 2.6 MW, as expected. It is confirmed by the PTO power curve, which is null for ME speed below 45 rpm, as expected. Figure 22 and Figure 23 show the ME fuel consumption rate and the ME consumption, respectively with PTO and without it. It can be observed that the highest consumption rate is obtained in case of not adoption of the PTO, while the lowest is obtained in case of the adoption of PTO with rated power of 2,6 MW followed by that with rated power of 1 MW. After a two-year time interval, the density of the MDO is assumed to be equal to 870 kg/m. The integration of the PTO implies an overall increase of the ME fuel consumption by 0.41 Ml corresponding to 0.36 MKg (360 t). Figure 24 and Figure 25 show the DE and load power, obtained respectively in the cases of adopting PTO and not adopting it. Figure 24 shows that the DE1 power alone covers the load power for ME speeds below 45 rpm, while it integrates the PTO power when the load power is higher than that produced by the PTO. The DE1 power is null when the load power

is entirely covered by the PTO. This happens in cruise mode for ME speeds above 45 rpm. Figure 25, on the contrary, shows that in the current working situation, the load power is shared, without any optimization, among two or three DEs. Figure 26 and Figure 27 show the DE fuel consumption rate and the DE consumption, respectively with PTO and without it. It can be observed that the consumption rate in case of adoption of the PTO is higher than that in its absence. After a two-year time interval, assuming a density of the HFO equal to 991 Kg/m^3, the integration of the PTO implies an overall decrease of the DE fuel consumption of 0.47 Ml corresponding to 0.47 MKg (470t). It should be noted that, while the net achievable reduction of fuel consumption is not significant in terms of volumes, it appears significant in terms of weight of fuel, given the different densities of MDO and HFO.

To pass from the fuel consumptions to the pollutant emissions, the coefficients provided in [10] have been used. Figure 28 and Figure 29 show the tables of the ME and DE polluting emissions, dividing them in NO_x, CO, SO_x, $PM_{2.5}$, CO_2 CH_4 and NO_2. It can be easily observed that, after a 2-year interval, all pollutants produced by the ME increase, while all pollutants produced by the DE decrease.

Figure 30 shows the global percent reduction of each pollutant after a two -year interval obtained due to the integration of the PTO technology. It can be observed that the highest reduction is that of SO_x, at around 13 %, followed by $PM_{2.5}$, at around 5 %, and the CO, at around 3 %. Only NO_x presents a percentage increase due to the integration of PTO, equal to around 2 %.

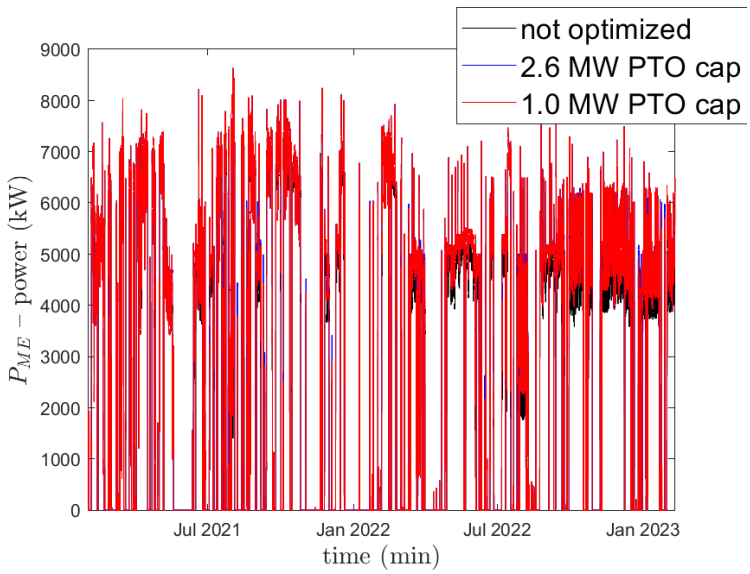

Figure 20: ME Power without and with PTO.

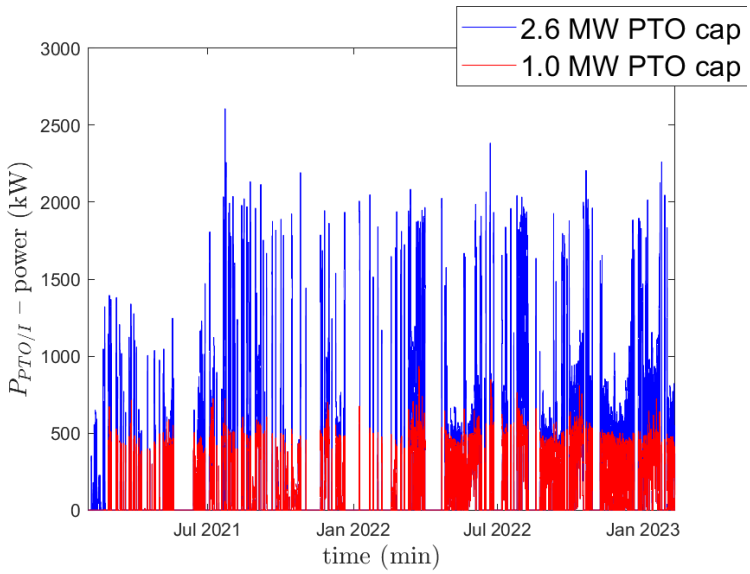

Figure 21: PTO power.

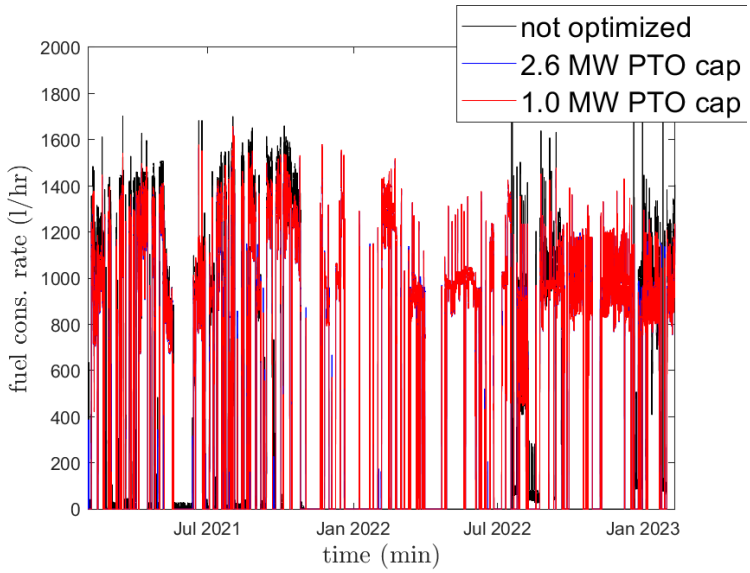

Figure 22: ME fuel consumption rate without and with PTO.

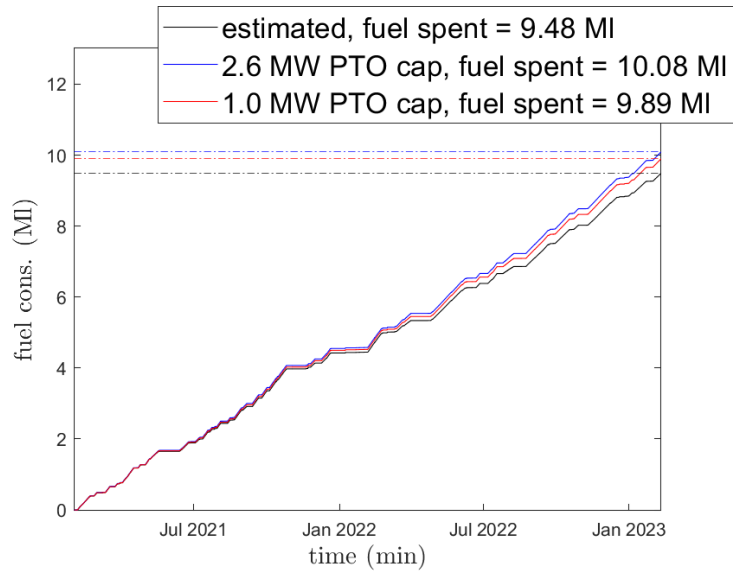

Figure 23: ME fuel consumption without and with PTO.

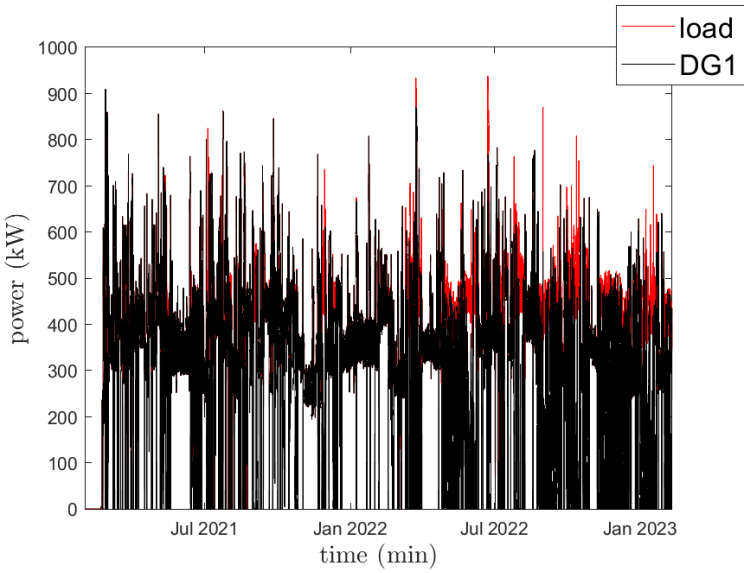

Figure 24: DE and load power with PTO.

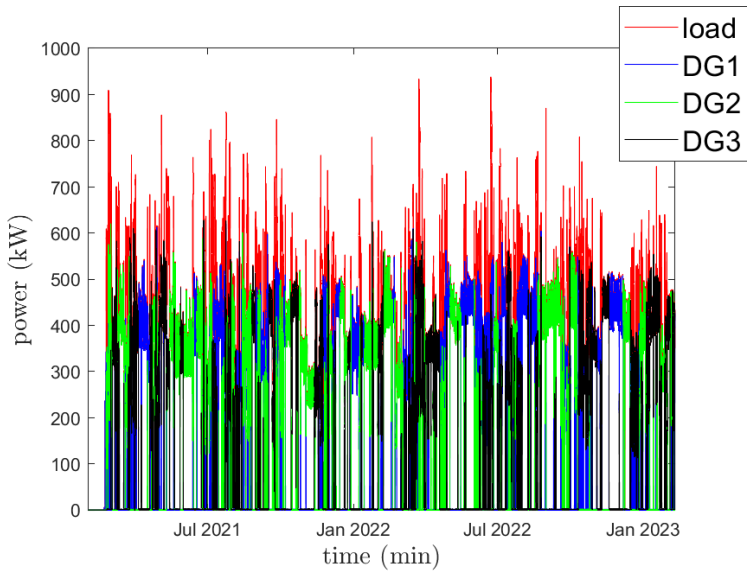

Figure 25: DE and load power without PTO.

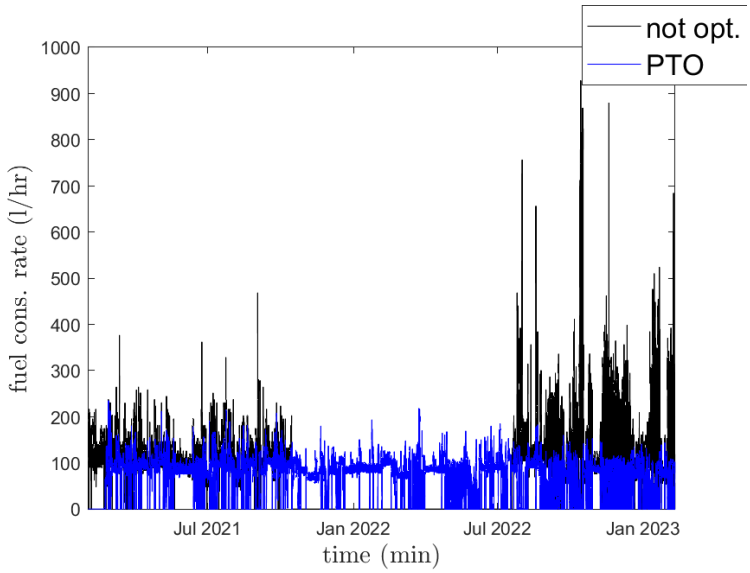

Figure 26: DE fuel consumption rate without and with PTO.

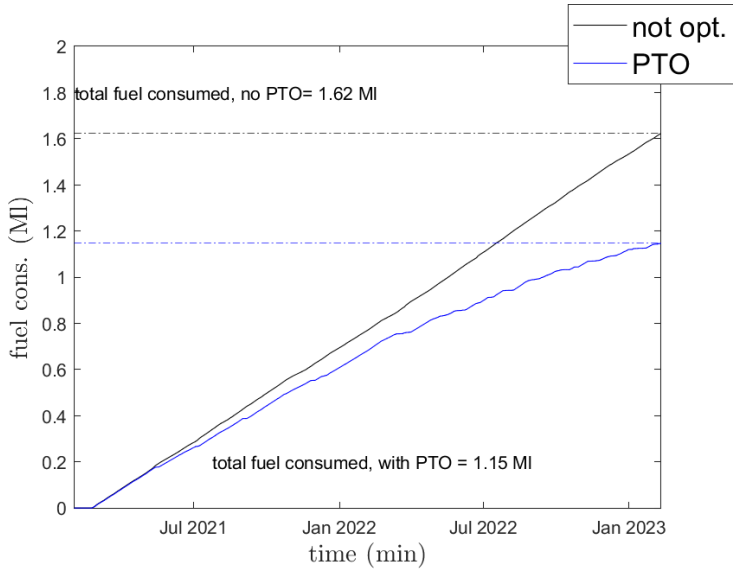

Figure 27: DE fuel consumption without and with PTO.

	not opt. (t)	PTO 1 MW cap (t)	Delta (t)
NOx	763.96	796.83	32.867
CO	22.553	23.523	0.97028
SOx	66.75	69.621	2.8717
PM2.5	9.0196	9.4076	0.38804
CO2	26525	27666	1141.1
CH4	0.27034	0.28197	0.01163
N2O	1.4017	1.462	0.060306

Figure 28. Overall polluting emissions by ME without and with PTO

	not opt. (t)	PTO 1 MW cap (t)	Delta(t)
NOx	91.67	64.787	-26.882
CO	5.8274	4.1185	-1.7089
SOx	68.313	48.28	-20.033
PM2.5	3.2716	2.3122	-0.9594
CO2	4721	3336.6	-1384.5
CH4	0.026137	0.018472	-0.0076648
N2O	0.20345	0.14379	-0.059663

Figure 29: Overall polluting emissions by DE without and with PTO.

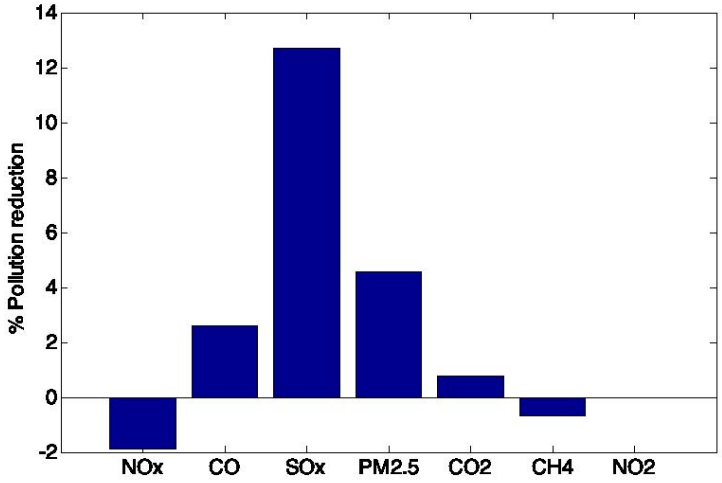

Figure 30: Overall percent polluting emission deduction by the integration of PTO.

6.2 Integrated PV system: Calculation of fuel savings for the Auxiliary Diesel Engine and emissions reductions

The integration of an onboard PV generator, as previously noted, impacts only the ship's auxiliary power. Therefore, the impact of the integrated PV system on ship efficiency and sustainability is measured in terms of fuel savings and emission reductions for the auxiliary diesel engine. This section presents the results of such an analysis conducted on the M/V Kastor ship.

The analysis aimed at evaluating the PV energy production during a reference time to assess the portion of auxiliary energy produced alternatively with respect to the use of electric diesel generators. This result allowed us to evaluate the corresponding fuel-savings (*FS*) and emission reduction (*ER*) as follows:

$$FS\ (tonnes) = SFOC_{AE} \cdot E_{PV} \cdot 10^{-6} \quad (19)$$

$$ER\ (tonnes) = e_i \cdot E_{PV} \cdot 10^{-6} \quad (20)$$

where:

- $SFOC_{AE}$ (g/kWh) is the average specific fuel oil consumption of the auxiliary engines (in our case study it is assumed to be equal to the declared SFOC at 50% of MCR of a single AE, given that the three AEs are of the same model and produced by the same manufacturer, i.e., 215 g/kWh),
- E_{PV} (kWh) is the energy produced by the PV array in the reference time,
- e_i (g/kWh) is the emission factor obtained from Cooper and Gustafsson according to the so-called "EP method" [15].

The index "*i*" in the emission factor refers to different pollutants, such as CO_2, SO_x, NO_x, and so on. The values of emission factors per pollutants of HFO (supplied to the auxiliary engines in our case study) are given in Table 8 [15].

Table 8: Emission factors per pollutant of HFO (EP method)

Pollutant	CO_2	SO_x	NO_x	CO	PM
Emission factor [g/kWh]	722	10.4	14	0.9	0.5

The evaluation of PV energy production was based on Osterwald's method, described in the following in equation.

$$E_{PV} = \int \eta_{PV} \cdot S \cdot G \cdot \left(1 - 0.005(T_{cell} - 25)\right) \cdot \eta_{PC} \quad (21)$$

In the previous equation, G is the solar irradiation. η_{PV} and η_{PC} are the efficiencies of the PV field and the power balance of plant (BoP) including the power converter connecting the power source with the power grid, S is the surface of the PV field, and T_{cell} is the PV cell temperature in Celsius degrees, obtained as:

$$T_{cell} = T_e + \left(\frac{NOCT-20}{800}\right) \cdot G \quad (22)$$

where T_e is the environmental temperature, NOCT is the operating cell temperature under G=800 W/m^2, T_e= 20 °C and wind speed equal to 1 m/s.

As already clarified in deliverable D6.4, to properly estimate the PV production, it was necessary to proceed with an estimation of solar irradiation G.

It is appropriate to preface that the analysis was conducted in the scenario synthesized below.

- The shipboard PV system, designed according to the criteria explained in deliverable D6.4, is envisaged to operate in grid-connected mode without any ESS;
- A one-year window (reference period) of operational data was considered for the analysis, i.e. 01/01/2021-31/01/2021
- Although bulk carriers do not follow a predetermined route, it is assumed that the operational profile in the reference year is sufficiently representative of the ship's average operational profile
- Some data preprocessing (data filling, spike elimination) was carried out to make them usable for the analysis
- The docking and navigation conditions during the reference period were identified and studied both individually and cumulatively.

6.2.1 Port stops

During the reference year, the vessel under study alternates between periods of sailing and stationing in port in accordance with the noon reports provided by Laskaridis. It remains anchored in port for 192 days while it sails at sea for 173 days.

The noon reports also provide information on the port stay schedule of the ship under study for the reference year which is shown in Table 9.

Table 9: Port stops of M/V Kastor in the reference year

Port stop n.	Site	Month	N. of days	from	to
1	Brindisi	January	17	01/01/2021	17/01/2021
2	Port Cartier	February	4	01/02/2021	04/02/2021
3	Hamburg	February	5	21/02/2021	25/02/2021
4	Ust Luga	March	12	01/03/2021	12/03/2021
5	Rotterdam	March	6	18/03/2021	23/03/2021
6	Slite	March	5	27/03/2021	31/03/2021
7	Slite	April	2	01/04/2021	02/04/2021
8	Civitavecchia	April	6	17/04/2021	22/04/2021
9	Fusina	April	5	26/04/2021	30/04/2021
10	Fusina	May	1	01/05/2021	01/05/2021
11	Gibraltar	May	2	06/05/2021	07/05/2021
12	Port Cartier	May	12	20/05/2021	31/05/2021
13	Port Cartier	June	13	01/06/2021	13/06/2021
14	Dunkirk	June	6	25/06/2021	30/06/2021
15	Dunkirk	July	3	01/07/2021	03/07/2021
16	Murmansk	July	3	10/07/2021	12/07/2021
17	Rotterdam	July	3	19/07/2021	21/07/2021
18	Slite	July	3	25/07/2021	27/07/2021
19	Ust Luga	July	2	29/07/2021	30/07/2021
20	Eemshaven	August	8	05/08/2021	12/08/2021
21	Ust Luga	August	6	16/08/2021	21/08/2021
22	Jorf Lasfar	August	1	31/08/2021	31/08/2021
23	Port Kamsar	September	8	06/09/2021	13/09/2021
24	San Ciprian	September	4	21/09/2021	24/09/2021
25	Murmansk	October	3	02/10/2021	04/10/2021
26	Las Palmas	October	1	15/10/2021	15/10/2021
27	Porto do Acu	October	6	26/10/2021	31/10/2021
28	Porto do Acu	November	21	01/11/2021	21/11/2021
29	Itaguai	November	3	23/11/20021	25/11/2021
30	Pecem	December	9	01/12/2021	09/12/2021
31	Paulsboro	December	12	20/12/2021	31/12/2021
	Total		**192**		

Calculating the energy produced by the PV generation system during port stops is quite easy since it is based on solar irradiance data provided by the Photovoltaic Geographical Information System (PVGIS) [16], a service developed by the European Union and freely accessible (*https://re.jrc.ec.europa.eu/pvg_tools/en/*). It provides information on solar irradiation and photovoltaic system performance for any location in the world with the exception of the North and South poles. As an example, Figure 31 illustrates the user interface of the PVGIS service. Figure 32 and Figure 33 show the diagrams of monthly global horizontal irradiation and monthly average

temperature for the year 2021 extracted from PVGIS referred to one of the ports where the ship docks several times during the reporting year, i.e., the port of Slite in Sweden.

Once the monthly solar irradiation and average temperature, coming from the PVGIS-ERA5 database, were extracted by PVGIS for each of the sites where the ship remains docked in port, the PV energy produced at each of the port stops was calculated. For such a calculation, the PV panel and BoP efficiency were considered. Particularly, the forthcoming results refer to the PV panel model Solbian SP-44 Panel, whereas the efficiency of BoP was assumed to be equal to 90%.

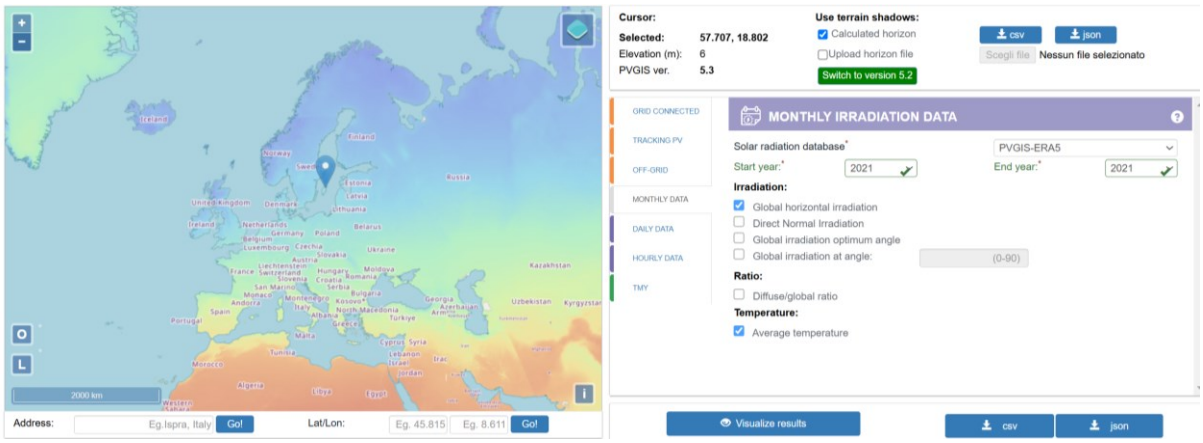

Figure 31: User interface of the PVGIS Service.

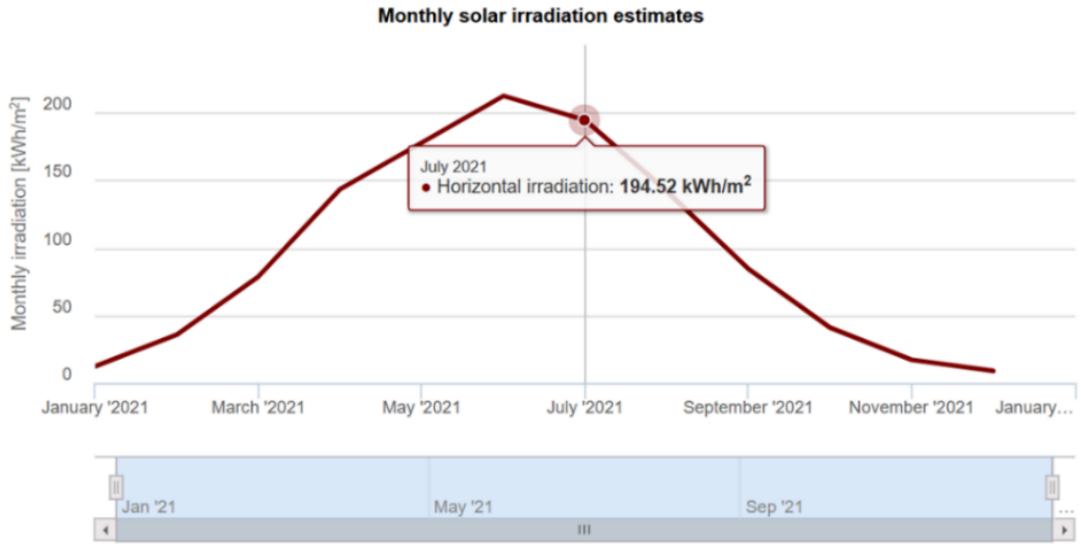

Figure 32: Monthly solar irradiation diagram for the year 2021 in Slite. Source: PVGIS-ERA5 database.

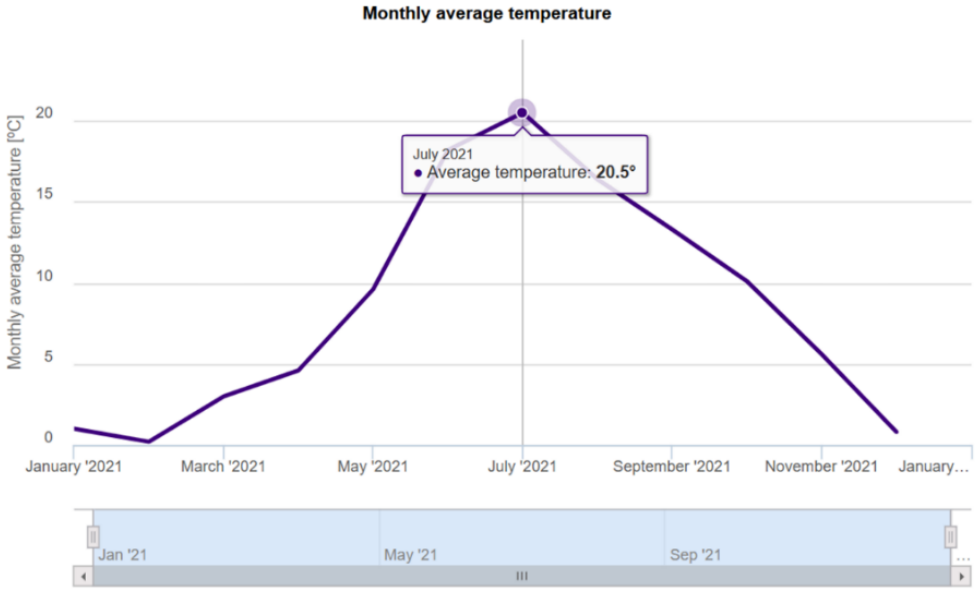

Figure 33: Monthly average temperature diagram for the year 2021 in Slite. Source: PVGIS-ERA5 database.

As far as the area of the PV field is concerned, the forthcoming results refer to situations where both hatch covers, and side walkways are exploited for PV panels' installation.

The description of different configurations of the PV field and related areas are recalled in Table 10, for the reader's convenience.

Table 10: Configurations for PV installations and related available areas.

Configuration	Description	Available area [m²]
"config_1_1"	PV panels installed on both hatch covers (helipad included) and side corridors	3,091
"config_1_2"	PV panels installed only on hatch covers (helipad included)	1,719
"config_2_1"	PV panels installed on both hatch covers (helipad excluded) and side corridors	2,858
"config_2_2"	PV panels installed only on hatch covers (helipad excluded)	1,486

It is worth noting that the possible configurations of the exposed PV array during port stop are the configurations identified as "config_1_2" and "config_2_2" in deliverable D6.4 and illustrated in Figure 34. As a matter of fact, during port stops, the hatch covers are supposed to be open. Therefore, even though PV panels are also meant to be installed on the side walkways (see 'config_1_1' and 'config_2_1' in deliverable D6.4), these areas end up being covered. As a result, the panels do not produce any power.

Finally, it is worth observing that any other scenario in terms of PV panel model selection and PV array configuration can be easily explored, based on the proposed approach.

The overall energy produced by the photovoltaic generator during port stops in the reference year was obtained by summing up the energy terms related to each port stop. The obtained value was 320,562 kWh for configuration "config_1_2" and 277,016 kWh for configuration "config_2_2". It was

also observed that these values barely deviate from those obtained by neglecting the temperature effect.

Based on the above values of E_{PV}, the following overall values of fuel saving were obtained: 68.92 t for configuration “config_1_2” and 59.55 t for configuration “config_2_2”. The corresponding emission reduction, in terms of different pollutants, were calculated as well considering the emission factors in Table 8; their values are given below in Table 15 and Table 16.

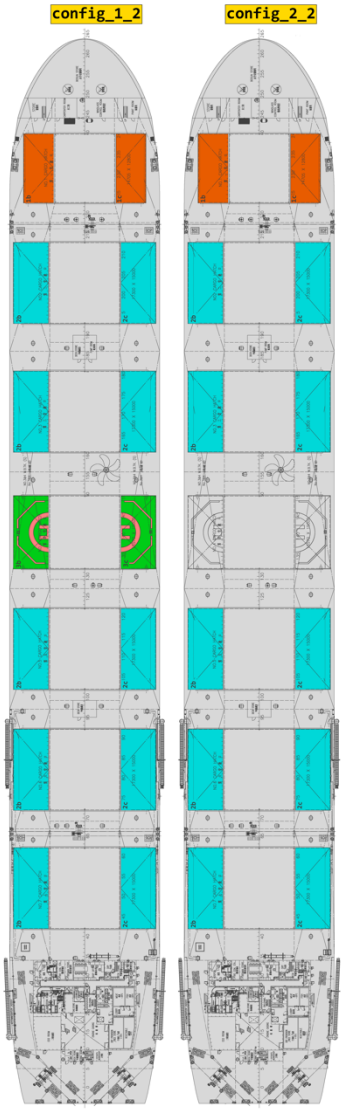

Figure 34: Exposed PV array during port stops.

6.2.2 Navigation

The method used to evaluate the reduction in fuel consumption of auxiliary engines and the corresponding reduction in pollutant emissions mirrors the approach followed in the case of port stops. However, unlike that case, there is no database available that provides monthly values of solar irradiation and temperature in the open sea. Therefore, it was chosen to calculate yearly energy

production from the PV generator using the value of average solar irradiance on the main global shipping route, equal to 200 W/m^2, as reported in the resolution IMO MEPC.351(78). This value is considered reasonable considering that it is very close to the mean value of average irradiances in the ports where the ship stops in the reference year (which span over a range of geographic regions from beyond the Arctic Circle to a latitude well below the equator) obtained by the PVGIS data, i.e. 189.4 W/m^2.

The duration of sailing periods and ports of departure and arrival are taken from the noon reports provided by Laskaridis. The schedule corresponding to the entire reporting year is given in Table 11.

Table 11: Navigation schedule of M/V Kastor in the reference year.

Navigation route n.	Departure/arrival port	Mont	N. of days	from	to
1	Brindisi - Port Cartier	January	14	18/01/2021	30/01/2021
2	Port Cartier -Hamburg	February	16	05/02/2021	20/02/2021
3	Hamburg - Ust Luga	February	3	26/02/2021	28/02/2021
4	Ust Luga - Rotterdam	March	5	13/03/2021	17/03/2021
5	Rotterdam -Slite	March	3	24/03/2021	26/03/2021
6	Slite - Civitavecchia	March	14	03/04/2021	16/04/2021
7	Civitavecchia -Fusina	April	3	23/04/2021	25/04/2021
8	Fusina – Gibraltar	May	4	02/05/2021	05/05/2021
9	Gibraltar - Port Cartier	May	12	08/05/2021	19/05/2021
10	Port Cartier - Dunkirk	June	11	14/06/2021	24/06/2021
11	Dunkirk - Murmansk	July	6	04/07/2021	09/07/2021
12	Murmansk - Rotterdam	July	6	13/07/2021	18/07/2021
13	Rotterdam -Slite	July	3	22/07/2021	24/07/2021
14	Slite -Ust Luga	July	1	28/07/2021	28/07/2021
15	Ust Luga - Eemshaven	July/August	5	31/07/2021	04/08/2021
16	Eemshaven -Ust Luga	August	3	13/08/2021	15/08/2021
17	Ust Luga - Jorf Lafar	August	9	22/08/2021	30/08/2021
18	Jorf Lasfar -Port Kamsar	September	5	01/09/2021	05/09/2021
19	Port Kamsar - San Ciprian	September	7	14/09/2021	20/09/2021
20	San Ciprian - Murmansk	September/October	7	25/09/2021	01/10/2021
21	Murmansk -Las Palmas	October	10	05/10/2021	14/10/2021
22	Las Palmas -Porto do Acu	October	10	16/10/2021	25/10/2021
23	Porto do Acu - Itaguai	November	1	22/11/2021	22/11/2021
24	Itaguai -Pecem	November	5	26/11/2021	30/11/2021
25	Pecem -Paulsboro	December	10	10/12/2021	19/10/2021
	Total		**173**		

The PV energy produced at each of the navigation routes was calculated in the same conditions assumed for the case of port stops, namely the PV panel model Solbian SP-44 Panel was selected and a BoP efficiency of 90% was assumed. Furthermore, once again, situations where both hatch covers and side walkways are exploited for PV panels' installation were considered. However, in this case,, the possible configurations of the exposed PV array were those identified as "config_1_1" and

"config_2_1" in deliverable D6.4 and shown in Figure 35 because the hatch covers are to be closed during navigation.

It is worth observing that any other scenario in terms of PV panel model selection and PV array configuration can be easily explored, based on the proposed approach.

The overall energy produced by the photovoltaic generator during navigation in the reference year was obtained by summing up the energy terms related to each navigation route. The obtained value was 589,103 kWh for configuration "config_1_1" and 544,594 kWh for configuration "config_2_1". Since an average temperature value is not available, the effect of temperature was neglected in this calculation, but it is believed that this does not significantly affect the obtained estimate.

Based on the above values of E_{PV}, the following overall values of fuel saving during navigation were obtained: 126.65 t for configuration "config_1_1" and 117.08 t for configuration "config_2_1". The corresponding emission reduction, in terms of different pollutants, were calculated as well considering the emission factors in Table 8. Their values are given below in Table 15 and Table 16.

6.2.3 Summary of efficiency performance of the PV generation system

Once the reduction in fuel consumption and pollutant emissions from the auxiliary diesel engines can be achieved through integrated photovoltaic generation on board the M/V Kastor ship during the port docking and sailing phases was quantified, it was possible to estimate the overall annual reduction in fuel consumption and pollutant emissions of the vessel.

In addition, using the operational data provided by Laskaridis, the consumption of the ship's auxiliary engines in current condition (i.e., in the absence of PV generators) and the impact of this retrofitting measure on the ship's efficiency and environmental sustainability are calculated.

The calculation of the ship's AEs fuel consumption expressed in mt/day was performed according to the following formula:

$$FC_{AEd} = (DG_{Inlet-FO-vol-flow-cons} - DG_{Outlet-FO-vol-flow-cons}) \cdot Density_{15°C-HFO} \cdot 24/1000$$

where the $DG_{Inlet-FO-vol-flow-cons}$ and $DG_{Outlet-FO-vol-flow-cons}$ are variables taken from the dataset provided by Laskaridis whose difference expresses the cumulated consumption of the three AEs in lt/h, and $Density_{15°C-HFO}$ is the density of HFO equal to 0.915 kg/l.

Based on such a calculation, an average fuel consumption of 2.4 mt/day is observed during the reference year (with an average fuel consumption of 2.2193 mt/day during the port stops and an average fuel consumption of 2.5697 mt/day during navigation).

By thoroughly knowing the schedule and duration of port stops and navigation routes, it was possible to calculate the consumption of AEs at individual stops and during navigation, as well as the total annual consumption for both port and navigation activities. The obtained results were: 414.5 mt in port and 440.7 mt in navigation.

Finally, by cumulating the estimated consumptions in port and navigation we obtained the overall estimate of AEs' annual consumption and consequently the overall estimate of pollutant emissions from them based on the emission factors reported in Table 8.

The summary of the obtained results, useful to assess the efficiency performance of shipboard integrated PV plants for the ship under study, are summarized in Table 12 and in Table 13 where the annual fuel consumption due to PV is indicated both in tons and in percentage of the fuel

consumption without any PV generator for the best and worst cases examined. To better clarify the means of best and worst cases, the “best case” refers to the PV array layouts including the hatch cover currently used as a helipad (i.e., “config_1_1” in navigation and “config_1_2” in port), whereas the “worst case” refers to the PV array layouts excluding the hatch cover currently used as a helipad (i.e., “config_2_1” in navigation and “config_2_2” in port).

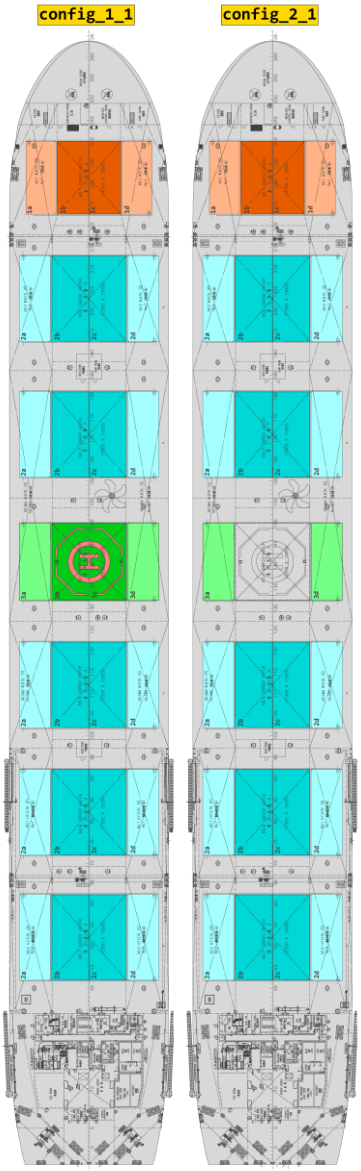

Figure 35: Exposed PV array during navigation.

Table 12: Annual efficiency performance of the PV plant in the “best case” scenario.

BEST CASE	Annual fuel consumption AEs [t] (NO PV)	Annual energy produced by PV [kWh]	Annual fuel saving due to PV [t]	Annual fuel saving due to PV [%]
Port	414.50	320,562	68.92	16.62
Navigation	440.73	589,103	126.65	28.73
Total	855.23	909,665	195.57	**22.86**

Table 13: Annual efficiency performance of the PV plant in the “worst case” scenario.

WORST CASE	Annual fuel consumption AEs [t] (NO PV)	Annual energy produced by PV [kWh]	Annual fuel saving due to PV [t]	Annual fuel saving due to PV [%]
Port	414.50	277,016	59.55	14.36
Navigation	440.73	544,594	117.08	26.56
Total	855.23	821,610	176.63	**20.65**

The effect on annual emission reduction of the PV plant in both the best- and worst-case scenarios were evaluated with reference to different pollutants, i.e., CO_2, SO_x, NO_x, CO, and $PM_{2.5}$. To do so, the annual emission per pollutant of the ship under study (as it is, namely without any PV generator) were calculated: the obtained values are reported in Table 14.

The annual emission reduction per pollutant due to the PV generator, expressed both in tons and in percentage terms with respect to the “NO PV ship” emission per pollutant, are reported in Table 15 for the best case scenario and in Table 16 for the worst case scenario.

Table 14: Annual emission per pollutant of the ship under study as it is (NO PV).

	Annual CO_2 emission (NO PV) [t]	Annual SO_x emission (NO PV) [t]	Annual NO_x emission (NO PV) [t]	Annual CO emission (NO PV) [t]	Annual PM emission (NO PV) [t]
Port	1317.72	19.07	25.59	1.63	0.91
Navigation	1401.10	64.45	27.21	1.73	0.97
Total	2718.82	83.52	52.79	3.36	1.88

Table 15: Emission reduction per pollutant due to PV generation (best case).

BEST CASE	CO_2 emission reduction due to PV		SO_x emission reduction due to PV		NO_x emission reduction due to PV		CO emission reduction due to PV		$PM_{2.5}$ emission reduction due to PV	
	[t]	[%]	[t]	[%]	[t]	[%]	[t]	[%]	[t]	[%]
Port	231.45	17.56	3.33	17.48	4.49	17.54	0.29	17.74	0.16	17.55
Navigation	425.33	30.36	6.13	9.51	8.25	30.32	0.53	30.66	0.29	30.34
Total	656.78	**24.16**	9.46	11.33	12.74	24.12	0.82	24.40	0.45	24.14

Table 16: Emission reduction per pollutant due to PV generation (worst case).

WORST CASE	CO_2 emission reduction due to PV		SO_x emission reduction due to PV		NO_x emission reduction due to PV		CO emission reduction due to PV		$PM_{2.5}$ emission reduction due to PV	
	[t]	[%]	[t]	[%]	[t]	[%]	[t]	[%]	[t]	[%]
Port	200.01	15.18	2.88	15.11	3.88	15.16	0.25	15.33	0.14	15.17
Navigation	393.20	28.06	5.66	8.79	7.62	28.02	0.49	28.34	0.27	28.04
Total	593.20	**21.82**	8.54	10.23	11.50	21.79	0.74	22.03	0.41	21.80

The comparison between the annual CO_2 emission of AEs without any PV plant and with PV plant (in both best and worst case scenarios) is also given graphically, in Figure 36. In addition, Figure 37 and Figure 38 illustrate respectively the emission reduction per pollutant due to PV (in tons) in the best case and worst case scenarios (a logarithmic scale on the y-axis was used to represent these quantities given the different order of magnitude of the emissions of the different pollutants). Finally, for completeness, the diagrams of fuel consumption per port stop (ps) and per navigation route (nr) with and without PV generation shown in Figure 39 and in Figure 40 provide more detailed information on the estimate of ship efficiency performance in the reference year selected for this analysis.

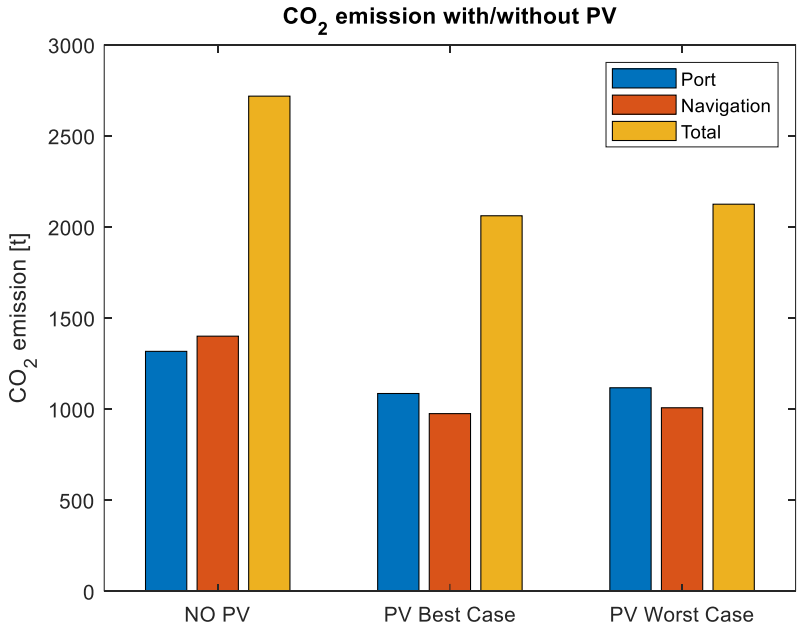

Figure 36: Comparison of the annual CO_2 emission of AEs with and without PV generation.

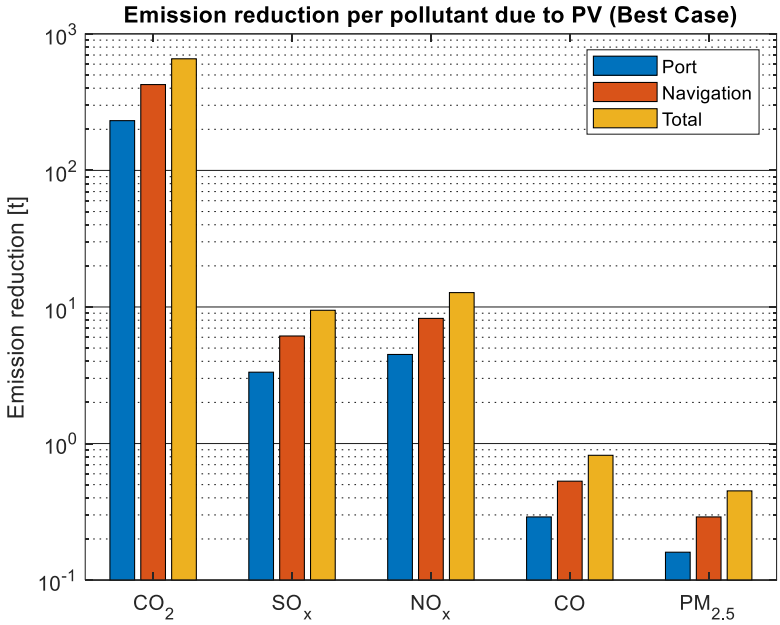

Figure 37: Emission reduction per pollutant due to PV in the best case scenario.

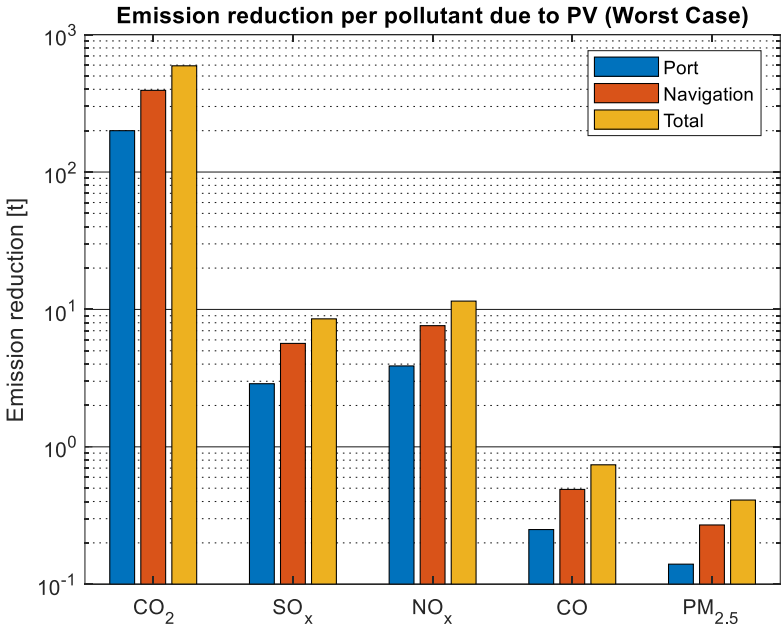

Figure 38: Emission reduction per pollutant due to PV in the worst case scenario.

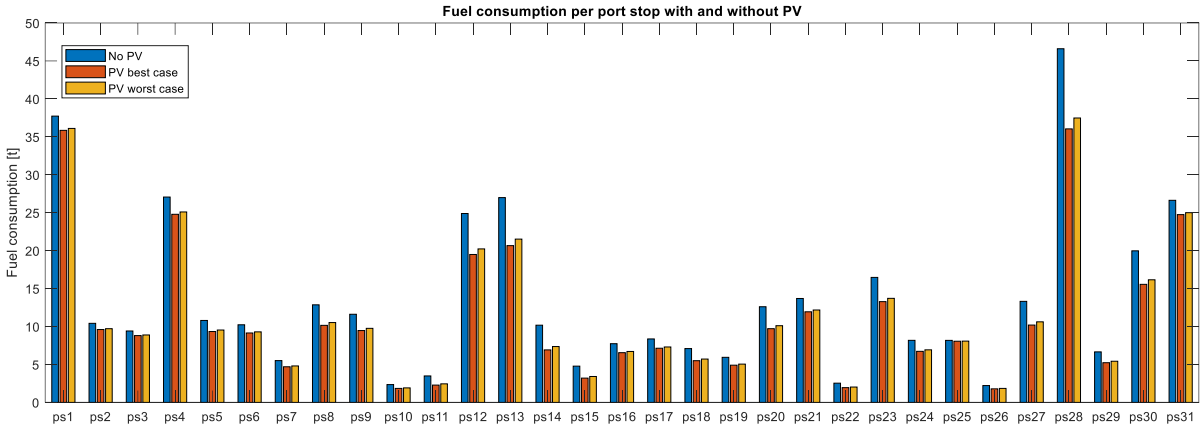

Figure 39: Fuel consumption per port stop with and without PV in the reference year (2021).

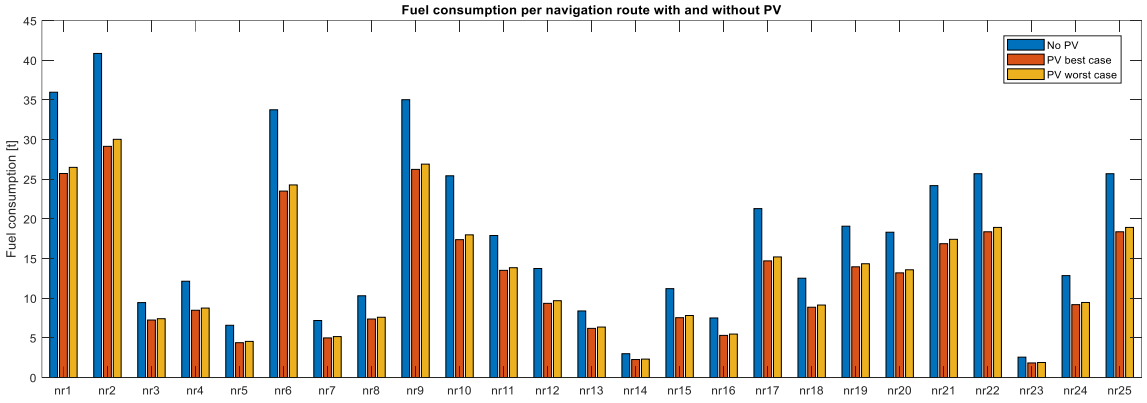

Figure 40: Fuel consumption per navigation route with and without PV in the reference year (2021).

The results coming from the above analysis clearly show the advantage of integrated PV generation in terms of fuel efficiency and emission reduction. As for fuel efficiency, it is possible to observe that the PV plant leads to an annual fuel saving going from 176.63 t (worst case) to 195.57 t (best case). This corresponds to an annual reduction in AEs fuel consumption going from 20,65% (worst case) to about 23% (best case).

This significant reduction in AEs' fuel consumption is reflected in a significant reduction of polluting emissions. As a matter of fact, a CO_2 emission reduction of about 22% to 24% is observed. Similarly, a reduction in emissions of the other pollutants considered (SO_x, NO_x, CO and $PM_{2.5}$) is noted in a range between 10% to 24%.

Since photovoltaic generation is an electrical retrofitting measure that only impacts auxiliary power, the improvements in efficiency and environmental sustainability resulting from this measure have been assessed so far only with reference to the auxiliary generators consumption and emission. To complete the analysis, we also aimed to evaluate the effect of photovoltaic generation on the overall fuel consumption and total emissions of the ship, including those from the main engine. Main engine fuel consumption in a two-year time span was already calculated, using the dataset provided by Laskaridis, in the part of the report dedicated to PTO. Its value is 9.48 Ml.

Consumption in the reference year is assumed to be half of that estimated in the two years, i.e. 4.74 Ml. From this figure, considering that the density of the MDO supplying the ME is 0.88 kg/l, the annual consumption of the ME in tons is obtained, which is 4,171.2 t. Consequently, the impact of PV on the overall ship's fuel consumption is computed in both the best- and worst cases, resulting in **3.89%** FC reduction in the best-case scenario and in **3.5%** FC reduction in the worst-case scenario.

Similar considerations can be extended to the estimation of emission reduction. As a matter of fact, the results presented so far considering such a reduction only referred to the AEs' behavior. If the emissions related to the ME are considered in the computation, the effect of PV generation on emission reduction (ER) is scaled accordingly, assuming the percentage amount synthesized in Table 17.

The emission per pollutant due to the ME were calculated considering MDO emission factors relating to the consumption of fuel with the emission of pollutants [15].

Table 17: Impact of PV generation on the whole ship's pollutant emissions.

	Annual CO2 emission [t]	**Annual SO_x emission [t]**	**Annual NOx emission [t]**	**Annual CO emission [t]**	**Annual PM emission [t]**
AEs	2718.82	83.52	52.79	3.36	1.88
ME	13260.24	33.36	381.91	11.27	4.5
Total (NO PV)	15979.06	116.88	434.7	14.63	6.38
ER due to PV (best-case)	4.11%	8.09%	2.93%	5.6%	7.05%
ER due to PV (worst-case)	3.71%	7.3%	2.64%	5.05%	6.4%

6.3 Performance of hybrid Fuel Cells/Battery/WHR systems

Figure 41 demonstrates the utilization hour distribution of the power generation or storage equipment in the scenario for the total operation time of 17,167.48 hours equivalent to 1.96 years.

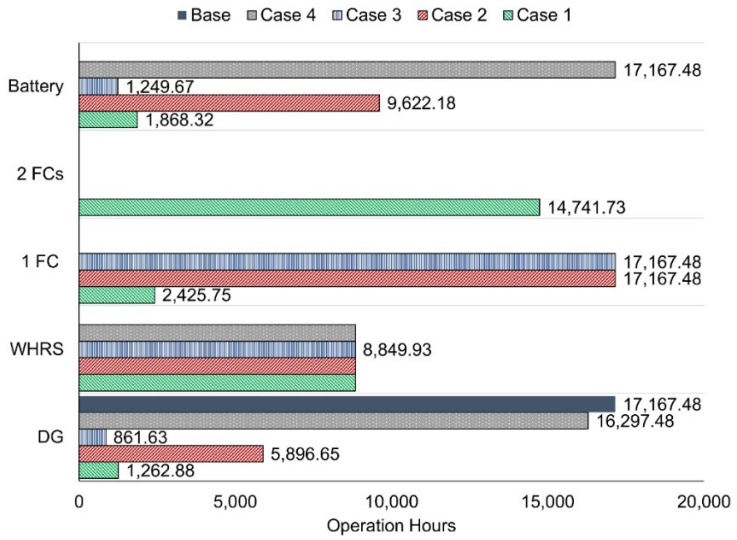

Figure 41: Usage hour distribution of equipment.

In the analyzed scenarios, the WHRS remained operational for a total of 8,849.93 hours. In Case 4, the combined use of the battery and WHRS led to a reduction in 870 hours of MDE operation. Case 1, characterized by the lowest FC power, achieved a 65.65% reduction in MDE utilization over the analyzed period. Meanwhile, Cases 2 and 3 provided reductions of 92.64% and 94.98%, respectively, in MDE usage. Battery utilization in Case 1 accounted for 56.05% of the total operation time, compared to 10.88% in Case 2 and 7.28% in Case 3. Notably, Case 1 predominantly operated with two FCs.

Table 18: Lifespan, total usage time, number of required renewals of FC and batteries.

Scenario	FC Lifespan (years)	Total FC Usage Time (h)	FC Renewal	Battery Lifespan (years)	Battery Renewal
Case 1	6.85	17,167.48	3	3.09	7
Case 2	4.91	31,909.22	5	10	2
Case 3	4.57	17,167.48	5	10	2
Case 4	N/A	N/A	N/A	1.94	11

Figure 41 shows the overall usage time of FCs, while Table 18 details the total FC running hours based on the distribution of active FCs. In Table 9, the estimated lifespan is capped at 10 years even if the usage exceeds this period. This means that any battery lifespan longer than ten years is assumed to require replacement at the ten-year mark.

Figure 42 illustrates the fuel consumption distribution across the scenarios during the 1.96-year operation period. The total FC usage time includes the parallel operating hours and is calculated by multiplying the number of FCs by their individual running hours.

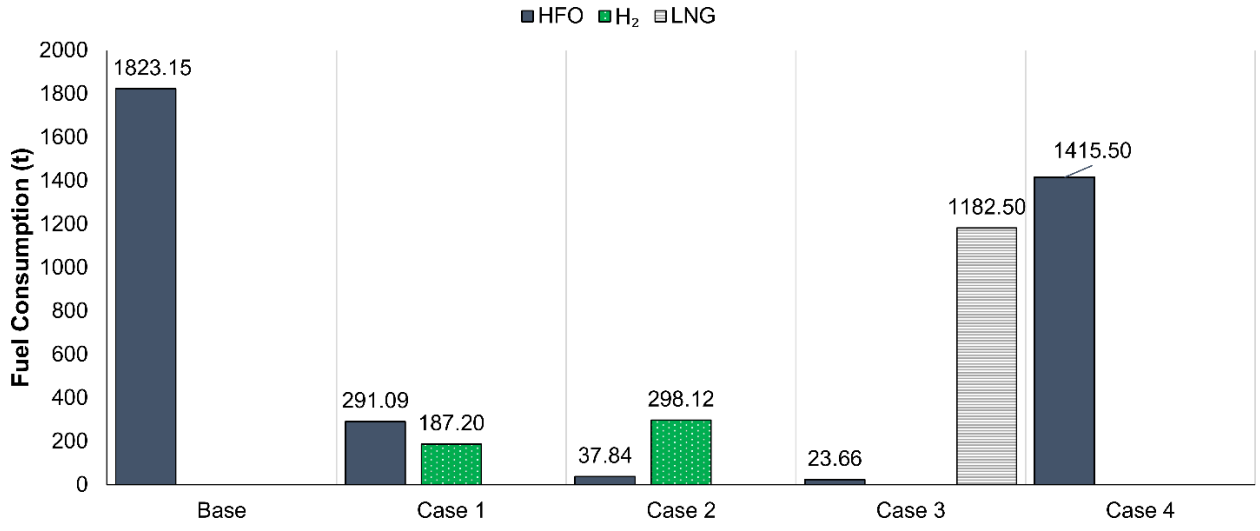

Figure 42: Fuel consumption distribution scenarios.

In the PEMFC and SOFC scenarios, fossil fuel usage could be almost zero. SOFCs consumed lower H_2 consumption compared to PEMFCs. Cases 1 and 2 provided 84.03% and 97.92% reductions in HFO usage of the plant. Case 3 cut the HFO utilization by 98.70% replacing it with LNG. Case 4 cut the HFO usage by 22.36%. The HFO tank capacity is 50.14% of the annual total consumption based on M/E and A/E data. A similar adjustment is assumed to be made for the HFO tanks for A/Es. Table 10 shows the calculated tank capacities for hybrid cases.

Table 19: Fuel tank capacities.

Capacity (m³)	Base	Case 1	Case 2	Case 3	Case 4
HFO	2738.30	2345.30	2280.33	2276.69	2646.86
H_2	0.00	393.00	457.97	0.00	0.00
LNG	0.00	0.00	0.00	461.61	0.00
Max. Utilization Days	183.01	95.73	70.05	105.96	189.33

In the base case scenario, the D/G fuel tank capacity is 467.68 m³. For each configuration, this capacity was reduced according to the fuel-saving ratios on HFO. Additional LNG and H_2 tanks were designed to replace D/G HFO storage. The volume of the H_2 tanks is based on compressed H_2, with a density of 75 kg/m³. In PAFC-utilized scenarios, less tank volume is needed since there is no requirement for H_2 storage. An onboard H_2 production facility could also decrease the required H_2 tank capacity for H_2-FC combinations. Figure 43 illustrates the operational/upstream $CO_{2\text{-eq}}$ and total reduction compared to the base scenario.

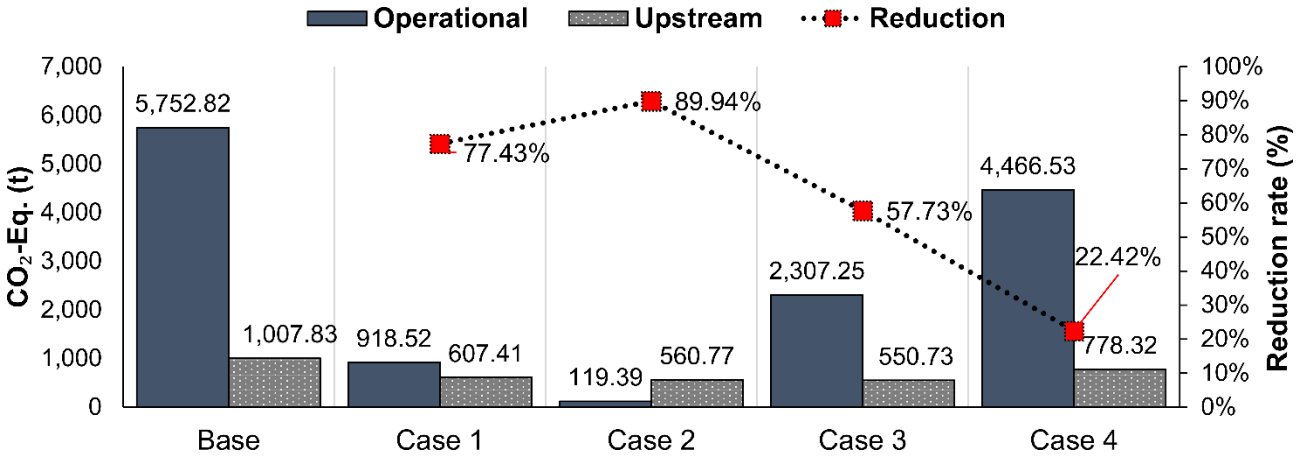

Figure 43: Operational and upstream $CO_{2\text{-eq}}$.

The left axis represents $CO_{2\text{-eq}}$ quantities, while the right axis displays reduction ratios. For example, Case 4 resulted in 4,466.53 tons (operational) and 778.32 tons (upstream) of $CO_{2\text{-eq}}$, achieving a total plant emission reduction of 22.42% resulting in a 3.79% reduction in the vessels' emissions. Case 2 achieved an 89.94% reduction in the plant's $CO_{2\text{-eq}}$ and a 15.21% reduction in the vessel's total $CO_{2\text{-eq}}$. In contrast, Case 1 reduced the plant's $CO_{2\text{-eq}}$ by 77.43% and the vessel's total $CO_{2\text{-eq}}$ by 13.10%. Case 3 achieved a 57.73% reduction in $CO_{2\text{-eq}}$, corresponding to 9.76% of the vessel's total $CO_{2\text{-eq}}$. Table 19 indicates the emissions from the remaining configurations.

Table 20: Other Emissions.

	Operational (t)				Upstream (t)			Total			
Scenario	NO_x	SO_x	PM	VOC	NO_x	SO_x	PM	NO_x	SO_x	PM	VOC
Base	1,646.31	45.58	5.07	5.62	16.46	4.65	0.11	1,662.77	50.23	5.18	5.62
Case 1	262.88	7.28	0.81	0.90	3.40	5.39	0.59	266.28	12.66	1.40	0.90
Case 2	34.17	0.95	0.11	0.12	1.27	5.67	0.69	35.44	6.62	0.79	0.12
Case 3	21.40	0.59	0.07	0.10	0.21	0.84	0.00	21.62	1.43	0.07	0.10
Case 4	1,278.20	35.39	3.94	4.36	12.78	3.61	0.09	1,290.98	39.00	4.02	4.36

The data highlights significant reductions in emissions across various scenarios compared to the base case. Case 3 exhibited the most substantial reductions, with total NO_x emissions reduced to 21.62 tons (a 98.70% reduction) and similarly low values for SO_x (1.43 tons), PM (0.07 tons), and

VOC (0.10 tons). Case 2 also performed exceptionally well, achieving total NO_x emissions of 35.44 tons (97.87% reduction) and notable decreases in SO_x (6.62 tons) and PM (0.79 tons). Case 1, while less effective, still achieved a total reduction in NO_x to 266.28 tons (83.99%) and moderate reductions in other pollutants. Case 4, by contrast, showed the least reduction overall, with total NO_x emissions at 1,290.98 tons, representing a reduction of only 22.36%, alongside proportionally smaller decreases in SO_x, PM, and VOC emissions. These results underscore the effectiveness of Cases 2 and 3 in minimizing emissions, particularly for NO_x, compared to the other scenarios. Figure 44 illustrates the attained versus required EEXI values across a base case and four subsequent cases.

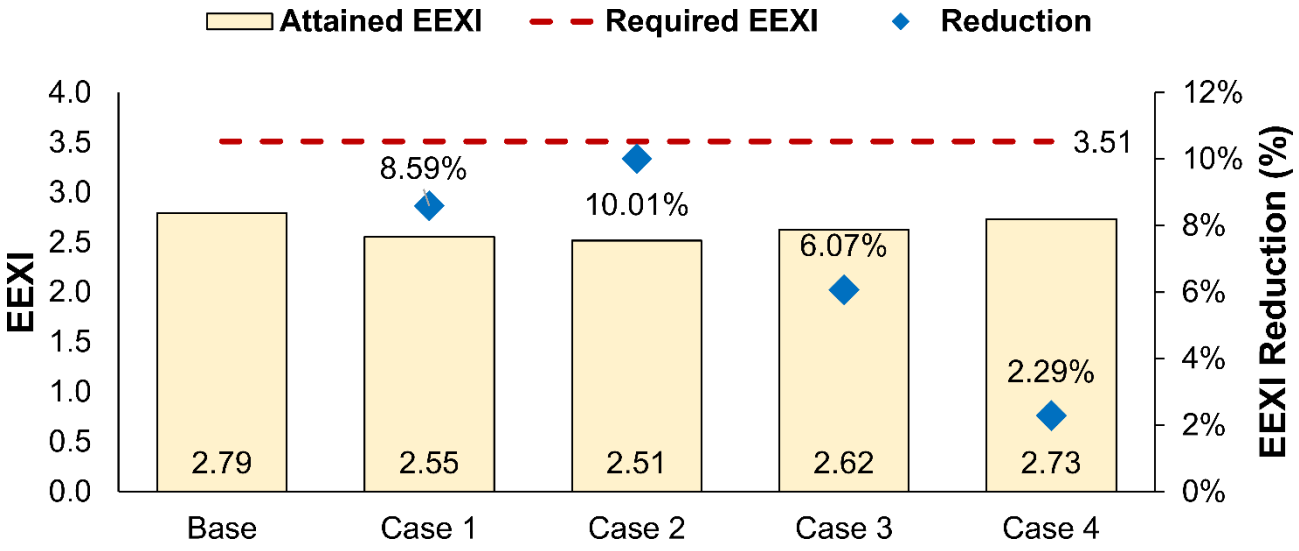

Figure 44: Attained and required EEXI.

Each case displayed both the EEXI attained by the vessels and the required EEXI to achieve compliance. The reduction percentage necessary for compliance was also highlighted for each scenario. Case 2 achieved the lowest EEXI, delivering a 10.01% reduction compared to the base configuration. In comparison, Case 1 demonstrated an 8.59% reduction, while Case 3 shows a 6.07% decrease. Case 4 ensured the lowest reduction of 2.29%.

7 Closing remarks

This document presents a comprehensive analysis of various electrification-based retrofitting solutions aimed at enhancing the energy efficiency and environmental performance of the M/V Kastor vessel through the implementation of innovative onboard microgrid architectures. The study focused on integrating key technologies such as PTO/PTI systems, PV panels, and FC/battery/ WHRS configurations, each contributing to reductions in fuel consumption and emissions in compliance with international regulatory frameworks.

The modified microgrid configurations examined here demonstrate that the PTO/PTI system, when properly designed, can slightly reduce the fuel consumption of the main engine, although the potential for fuel savings is limited due to inherent operational constraints. Notably, the PTO integration yields a net fuel consumption shift characterized by a moderate increase in main engine usage balanced by a more significant reduction in diesel engine consumption. This leads to a modest decrease in greenhouse gas emissions over a two-year period.

Conversely, the PV systems exhibit a more substantial impact on decreasing diesel engine fuel consumption and associated pollutant emissions, achieving more than a 20% reduction for the diesel engine segment annually. When accounting for the fuel consumption of the main engine, this translates into an overall yearly fuel consumption reduction of approximately 3.5–4% and a comparable reduction in CO_2 emissions.

An assessment of the FC/battery/WHRS hybrid solutions, extensively described in Deliverable D6.4, indicates promising performance in further reducing fuel consumption and emissions, thus reinforcing their potential as complementary retrofitting measures within the microgrid architecture.

Overall, the results affirm that the proposed retrofitting solutions hold significant promise for improving vessel efficiency and environmental sustainability. They merit further development and detailed investigation of PTO integration combined with energy storage systems in particular. This would be a key avenue for future project activities.

References

[1] J. Prousalidis, C. Patsios, F. Kanellos, A. Sarigiannidis, N. Tsekouras, and G. Antonopoulos, "Exploiting shaft generators to improve ship efficiency," in *2012 Electrical Systems for Aircraft, Railway and Ship Propulsion*, 2012, pp. 1–6. doi: 10.1109/ESARS.2012.6387443.

[2] J. ; X. E. ; V. K. Prousalidis, "Reactive power sharing in ship energy systems with shaft generators," *Journal of Marine Engineering & Technology* , vol. 8, no. 1, pp. 21–38, 2009.

[3] A. Sarigiannidis, A. Kladas, E. Chatzinikolaou, and C. Patsios, "High efficiency Shaft Generator drive system design for Ro-Ro trailer-passenger ship application," in *2015 International Conference on Electrical Systems for Aircraft, Railway, Ship Propulsion and Road Vehicles (ESARS)*, 2015, pp. 1–6. doi: 10.1109/ESARS.2015.7101529.

[4] A. G. Sarigiannidis, E. Chatzinikolaou, C. Patsios, and A. G. Kladas, "Shaft generator system design and ship operation improvement involving SFOC minimization, electric grid conditioning, and auxiliary propulsion," *IEEE Transactions on Transportation Electrification*, vol. 2, no. 4, pp. 558–569, Dec. 2016, doi: 10.1109/TTE.2016.2614999.

[5] M. C. Di Piazza, M. Pucci, and A. Iafrati, "Status and Future Trends of Electrification-Based Solutions for Efficiency-Oriented Ship Retrofitting," in *2024 IEEE International Conference on Electrical Systems for Aircraft, Railway, Ship Propulsion and Road Vehicles and International Transportation Electrification Conference, ESARS-ITEC 2024*, Institute of Electrical and Electronics Engineers Inc., 2024. doi: 10.1109/ESARS-ITEC60450.2024.10819870.

[6] ABB, "PTO/PTI, ENERGY EFFICIENCY HANDBOOK TOWARD ZERO EMISSION."

[7] MAN, "MAN B&W S60ME-C8.5-TII, Project Guide, Electronically Controlled Two-stroke Engines," Jul. 2018.

[8] MAN Energy Solutions, "Shaft generators for low speed main engines."

[9] M. Paulson and M. Chacko, "Marine Photovoltaics: A review Of Research And Developments, Challenges And Future Trends," *INTERNATIONAL JOURNAL OF SCIENTIFIC & TECHNOLOGY RESEARCH*, vol. 8, no. 09, 2019, [Online]. Available: www.ijstr.org

[10] C. Industry Committee of the IEEE Industry Applications Society, "IEEE Recommended Practice for Electrical Installations on Shipboard-Design IEEE Industry Applications Society," 2023. [Online]. Available: http://www.ieee.org/web/aboutus/whatis/policies/p9-26.html.

[11] P. Ghimire, M. Zadeh, S. Thapa, J. Thorstensen, and E. Pedersen, "Operational Efficiency and Emissions Assessment of Ship Hybrid Power Systems with Battery; Effect of Control Strategies," *IEEE Transactions on Transportation Electrification*, 2024, doi: 10.1109/TTE.2024.3365351.

[12] Y. Yuan, J. Wang, X. Yan, Q. Li, and T. Long, "A design and experimental investigation of a large-scale solar energy/diesel generator powered hybrid ship," *Energy*, vol. 165, pp. 965–978, Dec. 2018, doi: 10.1016/j.energy.2018.09.085.

[13] IMO, "MEPC.308(73) - 2018 Guidelines on the method of calculation of the Attained Energy Efficiency Design Index (EEDI) for new Ships," Oct. 2018.

[14] IMO, “MEPC.1/Circ.896, Guidance on treatment of innovative energy efficiency technologies for calculation and verification of the attained EEDI and EEXI,” Dec. 2021.

[15] L. Bilgili and U. B. Celebi, “Developing a new green ship approach for flue gas emission estimation of bulk carriers,” *Measurement (Lond)*, vol. 120, pp. 121–127, May 2018, doi: 10.1016/j.measurement.2018.02.002.

[16] “https://pvgis.com/.”